CHAPTER VII

ANALYSIS, INTERPRETATIONS AND CONCLUSIONS

7.1 GENERAL

The prime objective of the present investigation is to delineate mechanical behaviour of jointed rocks subjected to shear stress fields. It has been recognised that the behaviour does not conform to the classical behaviour of sliding between two rigid blocks depriving the benefit of classical mechanics and available mathematical models. Need therefore, is to develop a mechanistic model for the sliding process involved in jointed rocks and on which basis to formulate a mathematical model implementable through recognized numerical and computational methods in the engineering practice. To deduce the mechanistic concept it will be imperative to analyse and interprete the experiments conducted specifically to understand the fundamental aspects of sliding. In perspective of the expositions from the experimental observations the theoretical background is developed within the established frame work of mechanics. To test the validity and integrity of the theory it is essential to test it against the laboratory as well as field observations. Further, to establish the efficiency and efficacy of the mathematical model, it is obligatory to illustrate its utility in solving various engineering cases.

7.2 MECHANISTIC CONCEPT FOR SLIDING OF JOINTED ROCKS

7.2.1 The classical mechanism of friction between the two bodies assumed that the two bodies were rigid and the surfaces between the two bodies were absolutely plane involving no volume change, represented by saint venant body. It may be possible to generalise this classical model so as to incorporate variation in surface characteristics of the conventional nature owing to

alterations in physico-chemical structure of the surface. But when the surface variation is not only physico-chemical but also geometrical, it may not be possible to extend the classical laws of friction on simpler considerations. The process of sliding shall necessarily involve complex considerations. The prominent observations in the sliding of jointed rocks as depicted in the previous chapter indicate clearly that sliding between the jointed rocks cannot be considered analogous to the sliding between the two rigid bodies possessing plane surfaces. The significant difference between the two processes of sliding is change in bulk occurring on sliding surfaces in case of jointed rock vis a vis no bulk change in case of classical bodies. It can be conceived that the change in the bulk may be the result of continuous structural distortion of the sliding surfaces. Owing to this the initial characteristics of the jointed rock gets modified as a consequence of the process of sliding, rolling and crushing in addition to the physico-chemical variations of the surfaces. To describe the distortion integrally a parameter is required to be identified. In the current research practice this structural distortion is known in terms of dilation expressed in terms of deformation, in terms of energy or in terms of some mechanistic quantity. Physically it can be visualized as thickening between the sliding surfaces. The logical extension of the classical relation of friction - sliding friction - therefore, is to incorporate realistic parameter of dilation. One of the well recognised parameter in classical mechanics indicative of distortion is a non dimensional parameter in terms of strain ratio popularly known as Poisson's ratio. The value of the Poisson's ratio for no volume change is unity as assumed in classical frictional relationship. The classical relation for volume change can be :

$$\tau = f(\mu, \nu, \sigma) \qquad (7.1)$$

7.2.2 Though the classical laws of friction do not hold good for sliding of jointed rocks, however, the classical laws should

hold good for the instantaneous process of sliding between any sliding surfaces. Hence the sliding process in a jointed rock is analogous to sliding on resultant planes modifying continuously owing to the phenomenon of dilation. The sliding on number of resultant planes can be incorporated by an appropriate geometrical parameter. The phenomenological process of sliding in jointed rock is rather complex, since it involves varieties of phenomena taking place simultaneously during the movement on a plane. It is not feasible to quantify the phenomenological process of plastic sliding - elasto-plastic sliding-involving rolling, sliding and crushing processes and similar surface damage factors. To simplify this process an integral factor from laboratory observations may be identified to be incorporated in the classical laws of friction.

7.2.3 For unlubricated plane surfaces, values of Poisson's ratio are worked out at every stage of shear loading using equation 5.9. These values are tabulated in Table 7.1 to 7.3. Similar information for regularly aspereted surfaces are presented in Table 7.4 to 7.6. A typical set of calculations involved in working out Poisson's ratio from given values of normal and shear displacements corresponding to a given state of stresses is shown in Appendix-I.

Using the data from Table 7.1 to 7.6, plots of variation in Poisson's ratio ν versus variation in normal strain (εyy) are presented in Fig. 7.1 and 7.2 for the plane and aspereted surfaces respectively. These plots clearly indicate that value of Poisson's ratio is below unity when the joint is in the compressional mode, it invariably becomes unity when the joint starts opening mode and it goes on increasing further until a little earlier of the point of maximum normal strain, when it starts retarding towards unity. For an aspereted surface, this curve, as shown in Fig. 7.2, is a typical balloon type curve.

Variation of ν versus shear stress σxy is shown in

TABLE 7.1 : SAMPLE OF UNLUBRICATED PLANE SURFACE

Sample T_1B_1 Normal stress = σyy = 1.0 kg/cm^2 (constant)

Sr. No.	Shear stress 'σxy' in kg/cm^2	Normal strain 'εyy'	Shear strain 'γxy'	Shear strain 'εxy'	Poisson's ratio 'ν'
1	2	3	4	5	6
1	0.15	0.0020	0.025	0.012	0.85
2	0.29	0.0024	0.031	0.015	0.85
3	0.59	0.0024	0.041	0.020	0.89
4	0.74	0.0020	0.046	0.023	0.92
5	0.88	0.0012	0.053	0.026	0.98
6	0.95	0.0008	0.058	0.029	0.98
7	0.95	0.0004	0.066	0.033	0.99
8	0.91	0.0004	0.093	0.046	0.99
9	0.88	0.0000	0.121	0.061	1.00
10	0.85	-0.0008	0.127	0.064	1.01
11	0.79	-0.0008	0.130	0.065	1.01

TABLE 7.2 : SAMPLE OF UNLUBRICATED PLANE SURFACE

Sample T_2B_2 Normal stress = σyy = 1.5 kg/cm^2 (constant)

Sr. No.	Shear stress 'σxy' in kg/cm^2	Normal strain 'εyy'	Shear strain 'γxy'	Shear strain 'εxy'	Poisson's ratio 'ν'
1	2	3	4	5	6
1	0.15	0.0028	0.021	0.011	0.76
2	0.29	0.0032	0.027	0.013	0.78
3	0.44	0.0036	0.035	0.017	0.81
4	0.59	0.0044	0.041	0.020	0.81
5	0.74	0.0044	0.046	0.023	0.83
6	0.88	0.0044	0.053	0.026	0.85
7	1.03	0.0036	0.061	0.030	0.89
8	1.18	0.0028	0.069	0.035	0.92
9	1.33	0.0020	0.082	0.041	0.95
10	1.39	0.0012	0.110	0.055	0.98
11	1.43	0.0008	0.173	0.087	0.99
12	1.41	0.0000	0.188	0.094	1.00
13	1.38	-0.0004	0.204	0.102	1.00
14	1.35	-0.0004	0.212	0.106	1.00

TABLE 7.3 : SAMPLE OF UNLUBRICATED PLANE SURFACE

Sample T_3B_3 Normal stress = σyy = 2.0 kg/cm^2 (constant)

Sr. No.	Shear stress 'σxy' in kg/cm^2	Normal strain 'εyy'	Shear strain 'γxy'	Shear strain 'εxy'	Poisson's ratio 'ν'
1	2	3	4	5	6
1	0.15	0.0008	0.002	0.001	0.46
2	0.29	0.0012	0.006	0.003	0.57
3	0.44	0.0028	0.010	0.005	0.57
4	0.74	0.0036	0.017	0.008	0.64
5	1.03	0.0036	0.026	0.013	0.76
6	1.18	0.0028	0.030	0.015	0.83
7	1.47	0.0020	0.040	0.020	0.90
8	1.62	0.0012	0.046	0.023	0.95
9	1.77	0.0008	0.050	0.025	0.97
10	1.92	0.0004	0.056	0.028	0.98
11	1.98	0.0000	0.059	0.029	1.00
12	1.95	-0.0004	0.070	0.035	1.01
13	1.92	-0.0012	0.084	0.042	1.03
14	1.89	-0.0016	0.089	0.045	1.04
15	1.84	-0.0024	0.101	0.050	1.05
16	1.81	-0.0032	0.128	0.064	1.05

TABLE 7.4 : SAMPLE OF REGULARLY ASPIRATED SURFACE

Sample T_7B_7 Normal stress = σyy = 1.0 kg/cm^2 (constant)

Sr. No.	Shear stress 'σxy' in kg/cm^2	Normal strain 'εyy'	Shear strain 'γxy'	Shear strain 'εxy'	Poisson's ratio 'ν'
1	2	3	4	5	6
1	0.15	0	0.008	0.004	1.00
2	0.88	0	0.032	0.016	1.00
3	1.03	-0.0004	0.037	0.019	1.02
4	1.18	-0.0012	0.044	0.022	1.06
5	1.33	-0.0032	0.052	0.026	1.13
6	1.44	-0.0060	0.061	0.030	1.23
7	1.47	-0.0072	0.069	0.035	1.23
8	1.54	-0.0128	0.083	0.042	1.35
9	1.62	-0.0192	0.102	0.051	1.45
10	1.73	-0.0232	0.030	0.056	1.51
11	1.77	-0.0280	0.129	0.065	1.55
12	1.92	-0.0328	0.148	0.074	1.55
13	2.06	-0.0448	0.183	0.091	1.62
14	2.26	-0.0460	0.190	0.095	1.62
15	2.36	-0.0472	0.197	0.099	1.61
16	2.50	-0.0540	0.216	0.108	1.64
17	2.41	-0.0592	0.228	0.114	1.67
18	2.36	-0.0644	0.240	0.120	1.70
19	2.36	-0.0736	0.264	0.132	1.73
20	2.30	-0.0784	0.274	0.137	1.76

contd...

TABLE 7.4 (contd...)

1	2	3	4	5	6
21	2.26	-0.0876	0.296	0.148	1.79
22	2.21	-0.0924	0.307	0.154	1.81
23	2.06	-0.1028	0.333	0.166	1.84
24	1.92	-0.1056	0.338	0.169	1.85
25	1.77	-0.1076	0.343	0.171	1.85
26	1.62	-0.1104	0.350	0.175	1.85
27	1.47	-0.1124	0.358	0.179	1.85
28	1.33	-0.1136	0.370	0.185	1.83
29	1.18	-0.1136	0.385	0.192	1.79
30	0.59	-0.1056	0.437	0.214	1.61

TABLE 7.5 : SAMPLE OF REGULARLY ASPIRATED SURFACE

Sample T_8B_8 Normal stress = σyy = 1.5 kg/cm^2 (constant)

Sr. No.	Shear stress 'σxy' in kg/cm^2	Normal strain 'εyy'	Shear strain 'γxy'	Shear strain 'εxy'	Poisson's ratio 'ν'
1	2	3	4	5	6
1	0.15	0.0016	0.005	0.002	0.45
2	0.44	0.0016	0.015	0.007	0.79
3	0.59	0.0020	0.021	0.010	0.82
4	1.03	0.0020	0.036	0.018	0.90
5	1.47	0.0020	0.052	0.026	0.93
6	2.21	0.0020	0.075	0.037	0.95
7	2.36	0.0012	0.083	0.041	0.97
8	2.51	-0.0024	0.092	0.046	1.05
9	2.65	-0.0056	0.106	0.053	1.11
10	2.80	-0.0196	0.142	0.071	1.31
11	2.95	-0.0344	0.186	0.093	1.40
12	3.10	-0.0404	0.203	0.101	1.48
13	3.24	-0.0440	0.216	0.108	1.49
14	3.33	-0.0488	0.228	0.114	1.53
15	3.10	-0.0520	0.239	0.119	1.54
16	2.95	-0.0608	0.265	0.132	1.58
17	2.80	-0.0752	0.309	0.155	1.62
18	2.65	-0.0800	0.322	0.161	1.63
19	2.51	-0.0852	0.337	0.168	1.65
20	2.36	-0.0896	0.350	0.175	1.66

contd...

TABLE 7.5 (contd...)

1	2	3	4	5	6
21	2.21	-0.0920	0.361	0.180	1.66
22	2.06	-0.0936	0.370	0.185	1.65
23	1.92	-0.0948	0.380	0.190	1.64
24	1.77	-0.0956	0.386	0.193	1.63
25	1.62	-0.0960	0.394	0.197	1.62
26	1.47	-0.0960	0.400	0.200	1.61
27	1.18	-0.0932	0.420	0.210	1.55
28	1.03	-0.0884	0.437	0.218	1.50
29	0.88	-0.0800	0.466	0.233	1.41
30	0.80	-0.0672	0.497	0.248	1.31
31	0.74	-0.0580	0.516	0.258	1.25
32	0.70	-0.0480	0.536	0.268	1.20
33	0.65	-0.0372	0.565	0.282	1.14

TABLE 7.6 : SAMPLE OF REGULARLY ASPIRATED SURFACE

Sample T_9B_9 Normal stress = σyy = 2.0 kg/cm^2 (constant)

Sr. No.	Shear stress 'σxy' in kg/cm^2	Normal strain 'εyy'	Shear strain 'γxy'	Shear strain 'εxy'	Poisson's ratio 'ν'
1	2	3	4	5	6
1	0.15	0.0024	0.016	0.008	0.74
2	0.59	0.0024	0.026	0.013	0.83
3	0.74	0.0028	0.029	0.014	0.83
4	1.47	0.0028	0.050	0.025	0.89
5	1.62	0.0024	0.055	0.027	0.91
6	1.77	0.0020	0.061	0.030	0.93
7	1.92	0.0004	0.065	0.032	0.99
8	2.06	-0.0004	0.070	0.035	1.01
9	2.21	-0.0008	0.075	0.037	1.02
10	2.36	-0.0008	0.079	0.039	1.02
11	2.51	-0.0012	0.084	0.042	1.03
12	2.65	-0.0012	0.090	0.045	1.03
13	2.80	-0.0016	0.097	0.048	1.03
14	2.95	-0.0020	0.104	0.052	1.04
15	3.10	-0.0028	0.110	0.055	1.05
16	3.24	-0.0036	0.116	0.058	1.06
17	3.39	-0.0064	0.138	0.069	1.10
18	3.54	-0.0152	0.163	0.082	1.20
19	3.69	-0.0184	0.179	0.089	1.22
20	3.83	-0.0208	0.191	0.095	1.24
21	3.98	-0.0224	0.193	0.099	1.25
22	4.13	-0.0268	0.219	0.110	1.27
23	4.28	-0.0296	0.228	0.114	1.29
24	4.36	-0.0324	0.239	0.120	1.31
25	4.24	-0.0392	0.252	0.126	1.36
26	4.09	-0.0404	0.255	0.127	1.37

contd...

TABLE 7.6 (contd...)

1	2	3	4	5	6
27	3.97	-0.0438	0.265	0.132	1.39
28	3.83	-0.0456	0.273	0.136	1.40
29	3.69	-0.0604	0.275	0.138	1.54
30	3.54	-0.0668	0.299	0.149	1.56
31	3.39	-0.0696	0.306	0.153	1.57
32	3.24	-0.0728	0.316	0.158	1.58
33	3.10	-0.0760	0.329	0.164	1.58
34	2.95	-0.0776	0.335	0.167	1.58
35	2.80	-0.0788	0.340	0.170	1.58
36	2.65	-0.0800	0.349	0.174	1.58
37	2.51	-0.0808	0.351	0.175	1.58
38	2.36	-0.0816	0.361	0.180	1.57
39	2.21	-0.0824	0.371	0.185	1.54
40	2.06	-0.0828	0.379	0.189	1.54
41	1.92	-0.0828	0.388	0.194	1.53
42	1.77	-0.0824	0.397	0.198	1.51
43	1.47	-0.0780	0.418	0.209	1.45
44	1.18	-0.0656	0.456	0.228	1.33
45	1.17	-0.0580	0.476	0.238	1.28

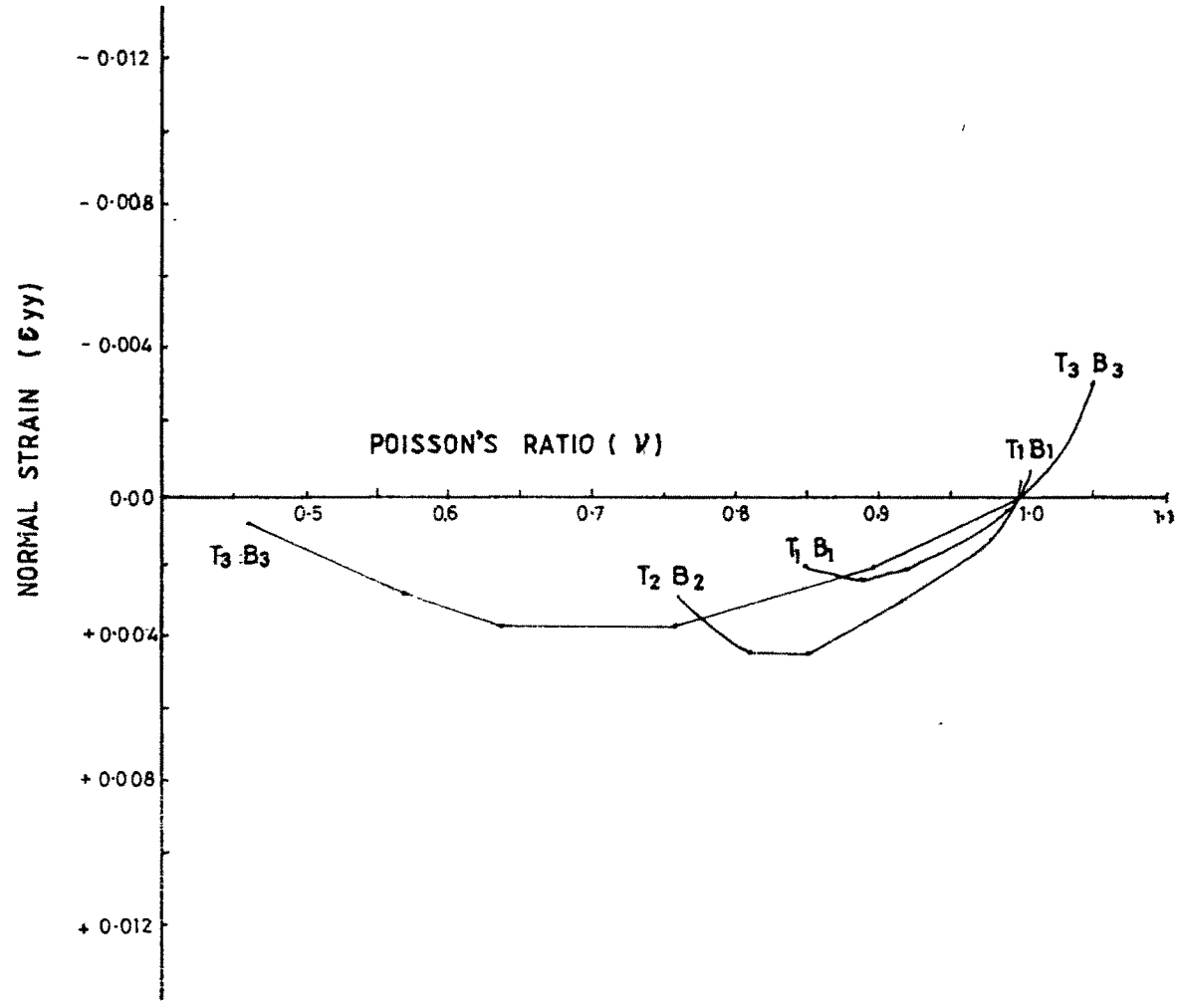

FIG: 7-1 VARIATION IN POISSON'S RATIO (ν) VERSUS NORMAL STRAIN(εyy)

- UNLUBRICATED PLANE SURFACES

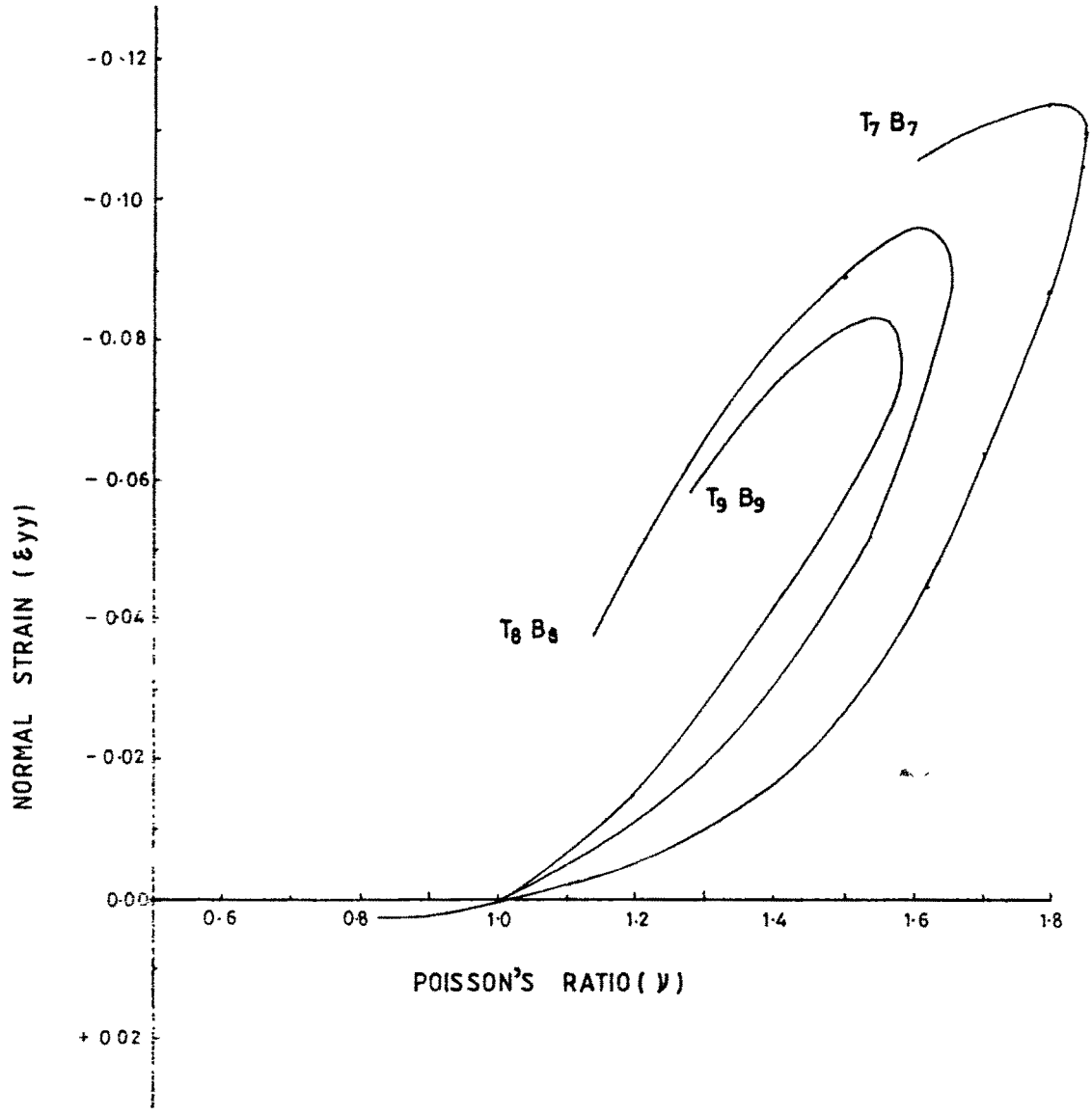

FIG:7·2 VARIATION IN POISSON'S RATIO (ν) WITH NORMAL STRAIN (εyy)

-REGULARLY ASPIRATED SURFACES

Fig. 7.3. The curve confirms that the Poisson's ratio continue to increase for some time beyond peak shear stress. Inverse of slope of this curve i.e. $d\nu/d\sigma xy$ is worked out at various points and is plotted versus corresponding shear stress as presented in Fig. 7.4.

7.3 GENERALISED FRICTION LAW

7.3.1 Failure envelopes of the unlubricated plane surfaces and surfaces having regular asperities (having asperity angle of 25°) are presented in Fig. 7.5. The failure envelope for the aspereted surfaces is non-linear while that for the unlubricated plane surfaces is a straight line, passing through origin. The envelope of the unlubricated plane surfaces can be represented by the relation,

$$\tau = \sigma \tan \phi_{\mu} \qquad (7.2)$$

where, τ = Shear Resistance
σ = Normal Stress
ϕ_{μ} = Basic friction angle

The failure envelope of the aspereted surfaces plotted in Fig. 7.5 gives the nature of the general equation of the curved failure envelopes in the form

$$\tau = K_1 \sigma^{K_2} \qquad (7.3)$$

where, K_1 = $\tan (\phi_{\mu} + i_o)$
K_2 = $\cos i_o$
i_o = average angle of asperity

Thus, the above relationship can be expressed as,

$$\tau = \sigma^{\cos i_o} \tan (\phi_{\mu} + i_o) \qquad (7.4)$$

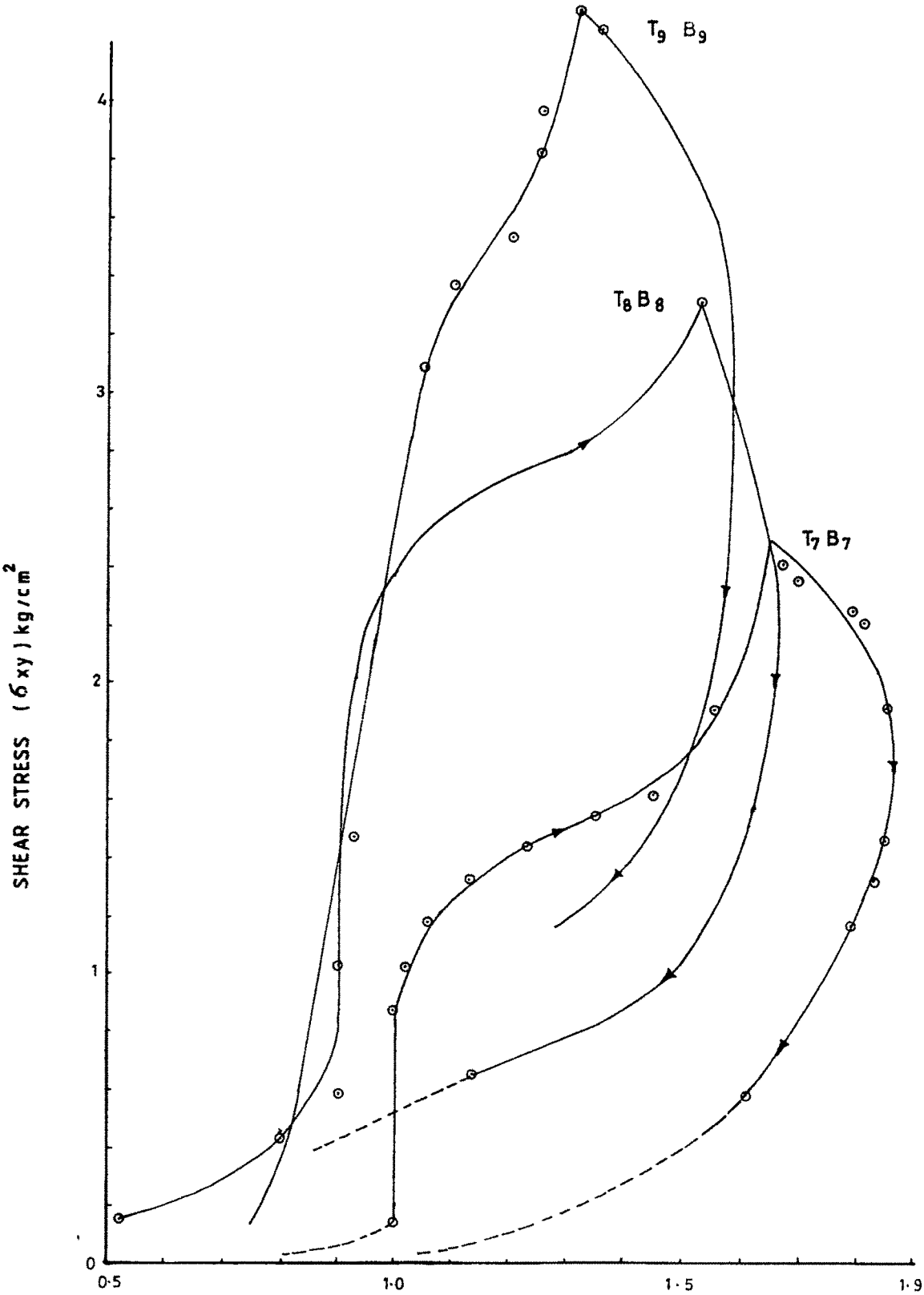

FIG: 7·3 VARIATION OF POISSONS RATIO (ν) VERSUS SHEAR STRESS (σxy)

– REGULARLY ASPIRATED SURFACES

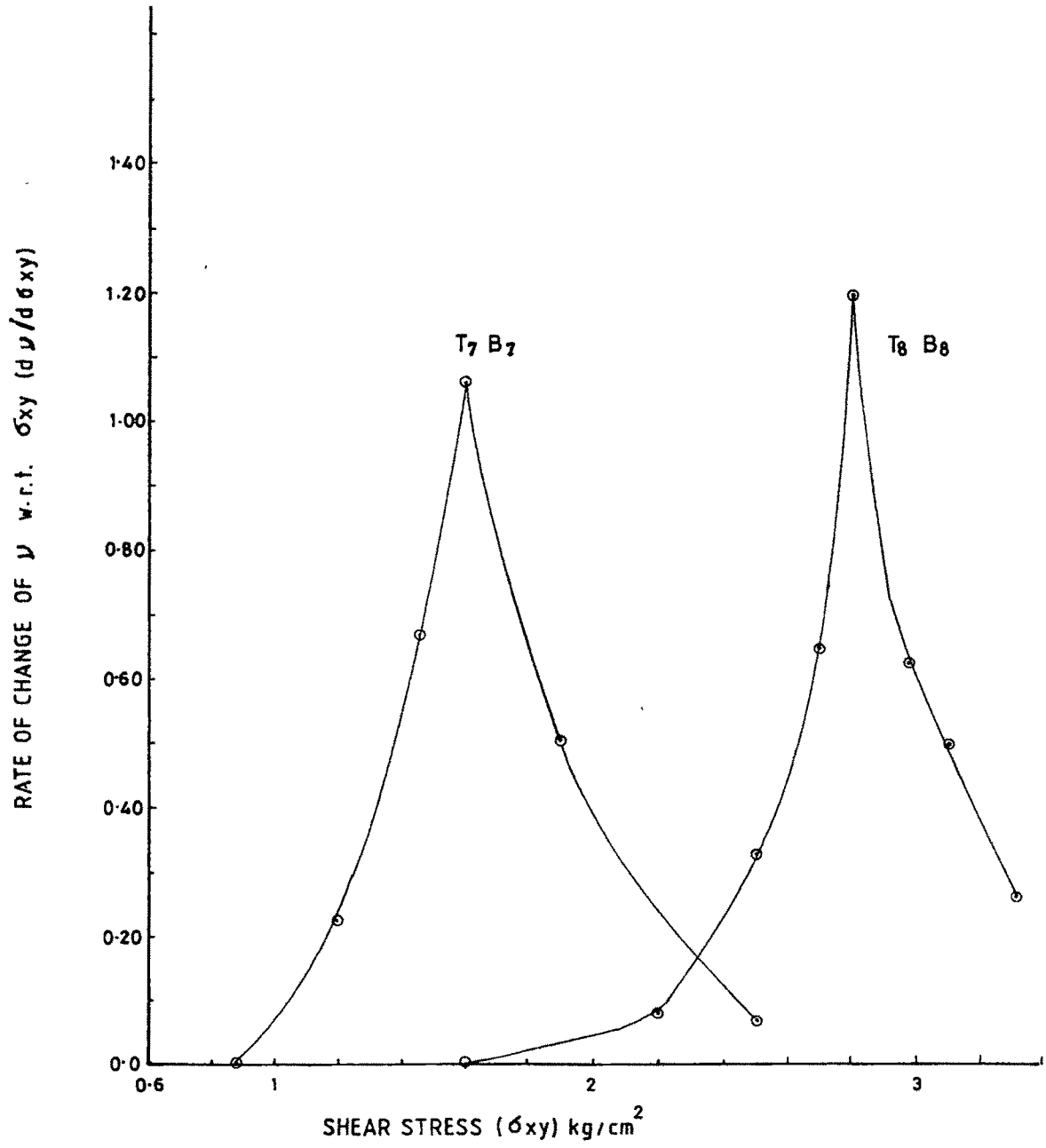

FIG: 7.4 VARIATION OF RATE OF CHANGE OF POISSON'S RATIO w.r.t. SHEAR STRESS ($d\nu / d\sigma xy$) VERSUS SHEAR STRESS (σxy)

-REGULARLY ASPIRATED SURFACES

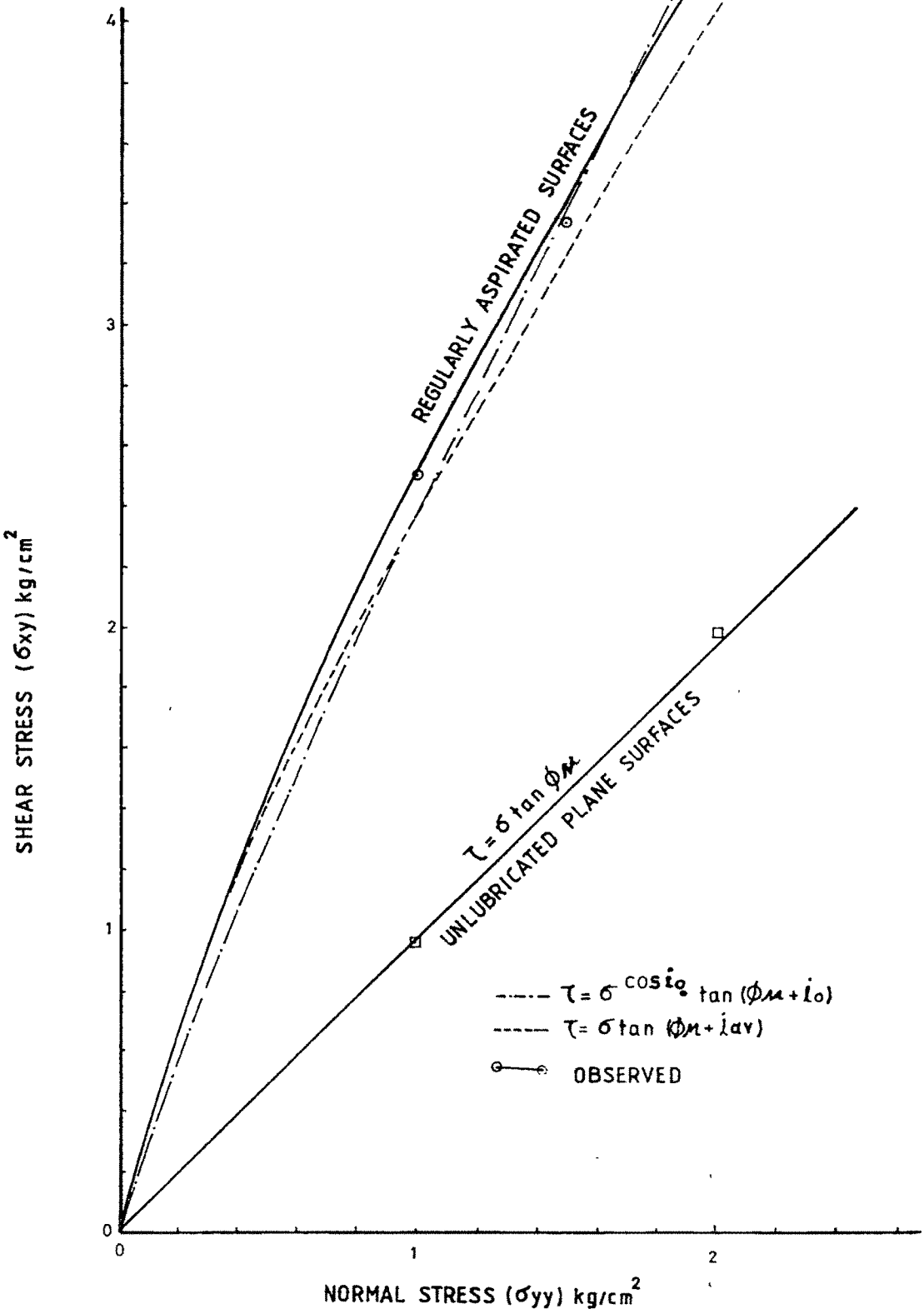

FIG: 7.5 COULOMB PLOTS FOR UNLUBRICATED PLANE AND REGULARLY ASPIRATED SURFACES

This is applicable to all types of surfaces with or without asperities. For plane surfaces putting $i_o = 0$ in the above equation, it reduces to the classical friction law.

$$\tau = \sigma \tan \phi_\mu \qquad (7.5)$$

The most significant exposition accruing from the equations 7.4 and 7.5 is that the asperity angle is a purely geometric parameter against dilation angle which is dependent on normal stress and therefore not a purely geometric parameter. Thus equation 7.4 is a general law of friction with the only modification of introduction of average angle of asperity (i_o) present on the sliding surfaces. It is easier to arrive at an average asperity angle for a given surface with the help of a profilometer. Thus equation 7.4 is a convenient form to handle with.

7.3.2 Another important fall out of the present investigation is that it is possible to estimate average dilation angle for the given normal stress. Comparing the dilation curves for different normal stresses (superimposed on an asperity) shown in Fig. 7.6, it is seen that the average dilation angle (i_{av}) decreases with increasing normal stress as the asperities are sheared through more and more. It is also seen that the average dilation angle (i_{av}) can be correlated with normal stress as shown in Fig. 7.7. This will take a form of

$$i_{av} = \frac{2}{3} i_o \cdot \sigma^{-K} \qquad (7.6)$$

Where, the power K is related as,

$$K = \tan^2 (45 - \frac{\phi_\mu}{2}) = \tan^2 \beta_c \qquad (7.7)$$

where, the angle $\beta_c = (45 - \frac{\phi_\mu}{2})$ is the critical direction of sliding which absorbs minimum energy in friction.

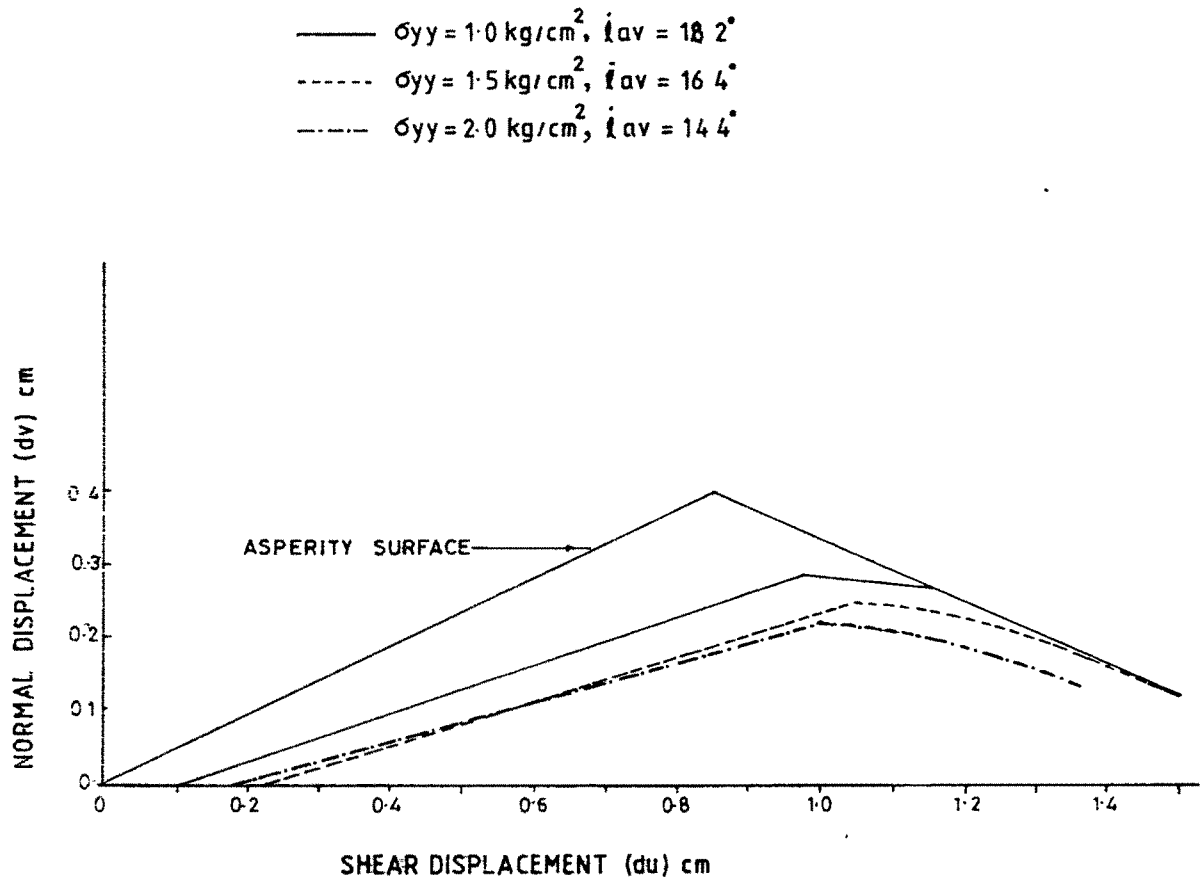

FIG:7·6 AVERAGE DILATION ANGLE (i_{av}) FOR DIFFERENT NORMAL STRESSES (σ_{yy})

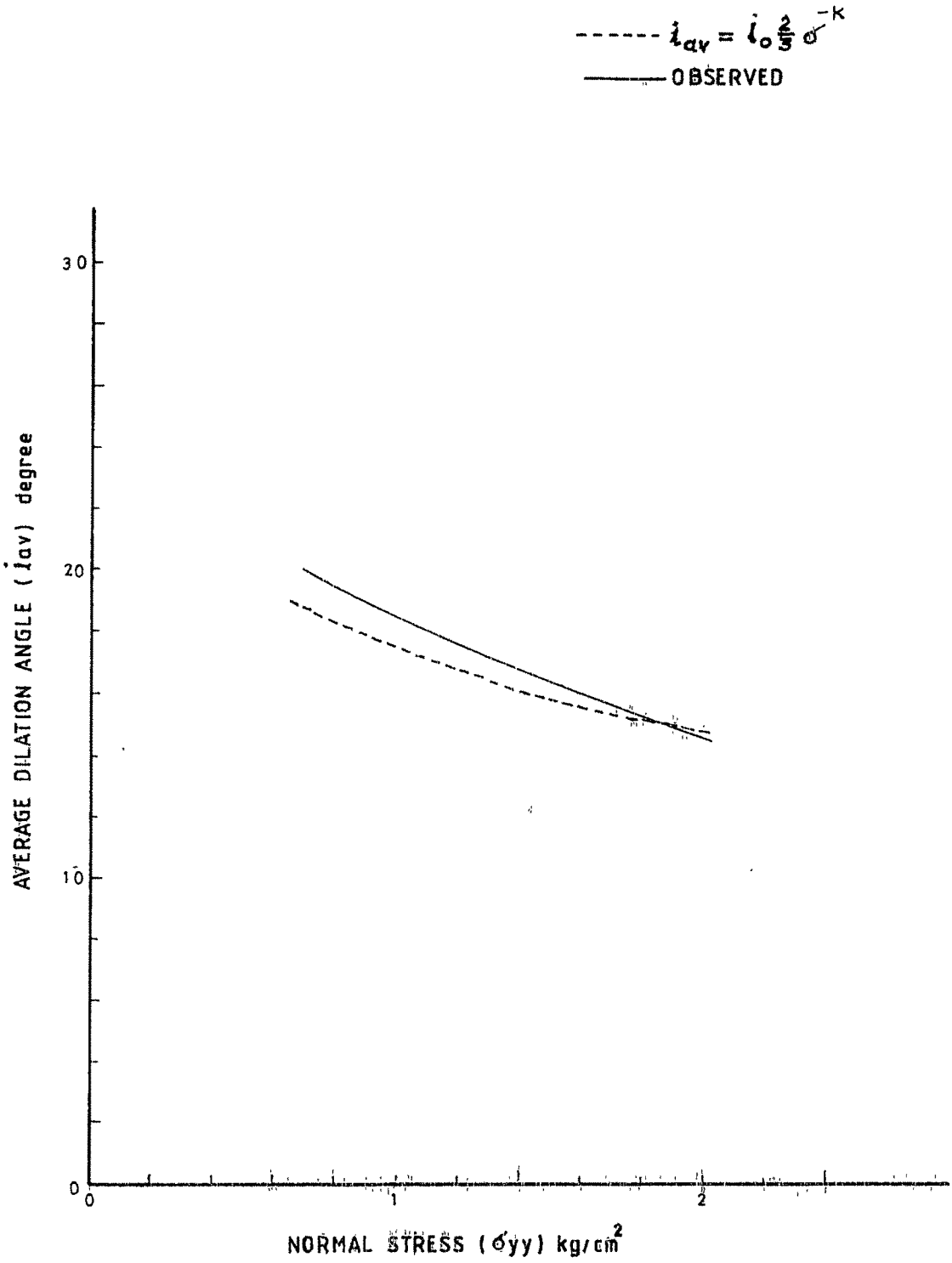

FIG: 7-7 RELATION BETWEEN AVERAGE DILATION ANGLE (i_{av}) AND NORMAL STRESS (σ_{yy})

7.3.3 Now, it is possible to propose a generalized friction equation with dilation parameter incorporating classical equation of friction for no volume change, as under :

$$\tau = \sigma \tan (\phi_\mu + i_{av}) \qquad (7.8)$$

or

$$\tau = \sigma \tan (\phi_\mu + \tfrac{2}{3} i_o \sigma^{-K}) \qquad (7.9)$$

If there is no volume change, i_{av} becomes zero, thereby degenerating the classical equation of friction.

Equation 7.4 and 7.9 are two alternative forms of general law of friction for jointed rocks incorporating average angle of initial asperity (i_o) and average dilation angle (i_{av}) respectively. The resulting failure envelopes are shown in Fig. 7.5.

7.4 CONSTITUTIVE MODELLING FOR THE JOINTED ROCKS

In order to translate the mechanistic model of sliding of jointed rock, a plausible amneable, mathematical model is required to be developed for its utilisation in understanding the various engineering situations with reference to jointed rocks. Any mathematical modelling, if it is to be valid, should conform the well established analytical systems.

It has been recognised that sliding behaviour in jointed rock can be explained by introducing a joint element in which the characteristics of a joint fully reflect. In the Chapter V a new joint element has been developed incorporating a structural parameter in terms of Poisson's ratio in its constitutive matrix. The matrix is as under :

$$[D] = \frac{1}{E} \begin{bmatrix} 1 & 0 & 0 \\ 0 & 1-\nu^2 & 1-\nu \\ 0 & 0 & 1+\nu \end{bmatrix} \qquad (7.10)$$

and

$$[D] = \frac{1}{E}\begin{bmatrix} 1 & 0 & 0 \\ 0 & 2D(1-\nu)(1+2\nu) & 0 \\ 0 & 0 & 1+\nu \end{bmatrix} \qquad (7.11)$$

The observed and predicted displacements for the aspereted samples tested are tabulated in Table 7.7. Fig. 7.8 to 7.10 are the typical plots showing the comparision of predicted and observed shear stress versus normal displacement curves. From these it is evident that the constitutive matrix of the joint element which has been developed during the present investigation reasonably predicts the experimental observations. Thus the joint element developed in the present investigation, provides a tool to investigate into the mechanical behaviour of jointed rocks.

7.5 MECHANICAL BEHAVIOUR OF JOINTED ROCK OBSERVED IN LABORATORY

7.5.1 Relationship between shear stress and shear strain of samples of regularly aspereted surfaces is presented in Fig. 7.11. It is seen that all samples indicate an initial shear modulus G equal to 25 kg/cm^2 which drops to 7 kg/cm^2 after certain shearing. The shear stress or the shear strain at which such a change occures depends upon the normal stress. Thus the shear stress-strain relationship of fig. 7.11 can be modelled by a bilinear model having equation,

$$\sigma_{xy} = 50\ \varepsilon_{xy} \ldots\ldots\ldots\ldots \text{ if } \varepsilon_{xy} \leqslant \varepsilon_{xyc} \qquad (7.12)$$

$$\sigma_{xy} = 50\ \varepsilon_{xyc} + 14\ (\varepsilon_{xy} - \varepsilon_{xyc}) \ldots \text{ if } \varepsilon_{xy} > \varepsilon_{xyc}$$

where, $\varepsilon_{xy} = \frac{1}{2}\gamma_{xy}$ and ε_{xyc} is the critical shear strain at which the slope of the curve changes. It can be specified as,

$$\varepsilon_{xyc} = 0{\cdot}05\ \sigma_{yy}^{1{\cdot}25} \qquad (7.13)$$

Alternatively, the corresponding critical shear stress σ_{xyc} can be specified as :

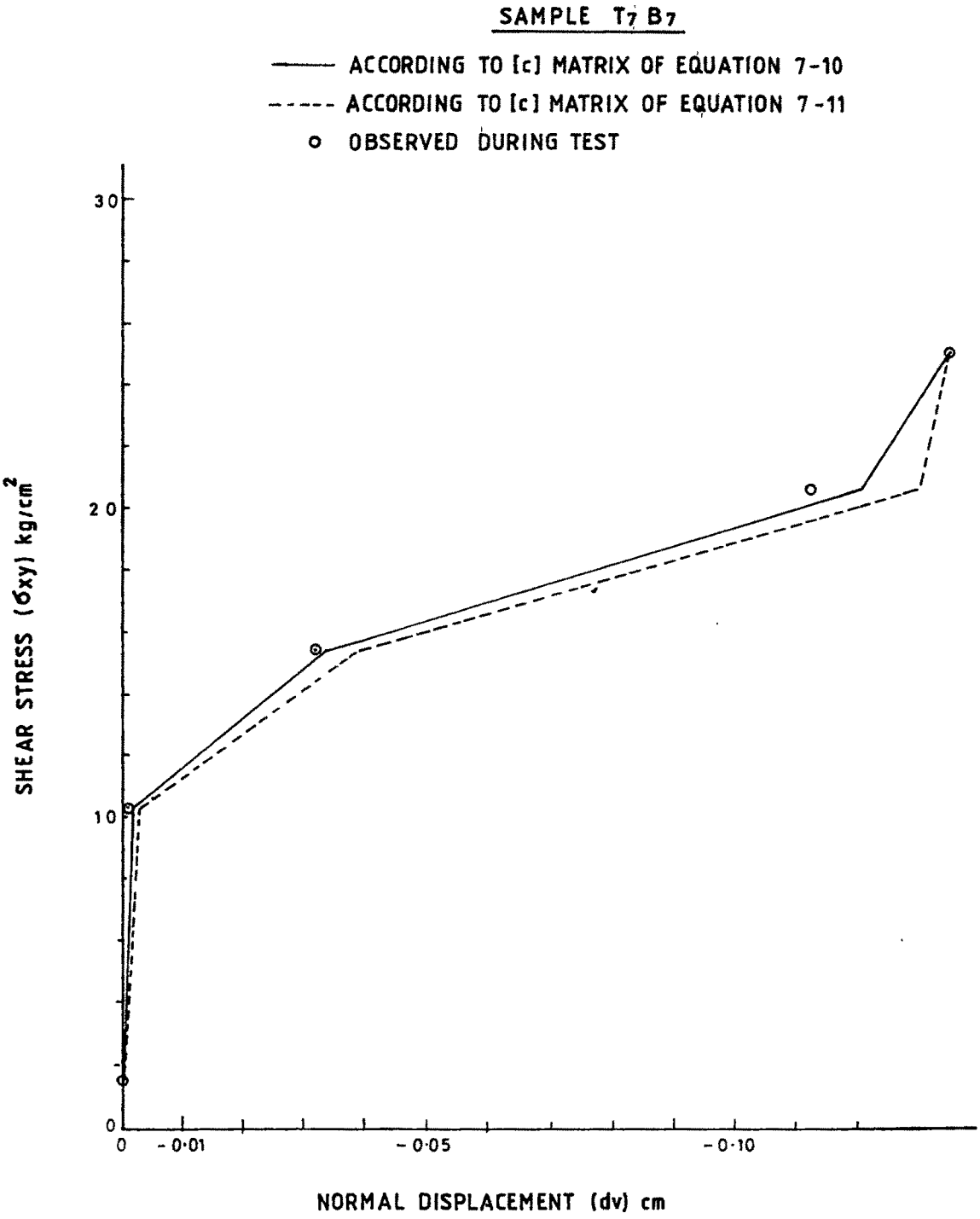

FIG: 7-8 COMPARISION OF OBSERVED AND PREDICTED DISPLACEMENTS - REGULARLY ASPIRATED SURFACES

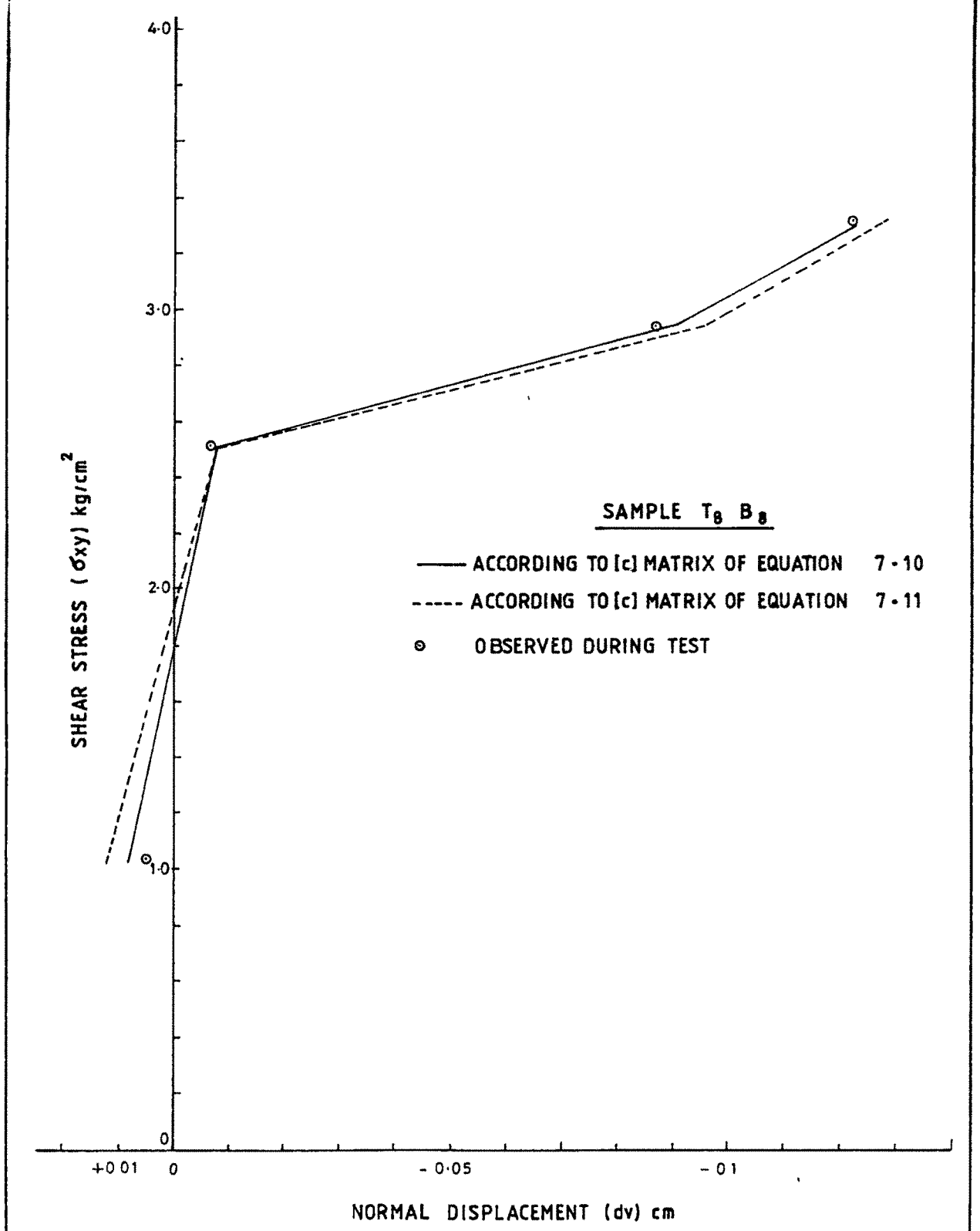

FIG: 7·9 COMPARISION OF OBSERVED AND PREDICTED DISPLACEMENTS - REGULARLY ASPIRATED SURFACES

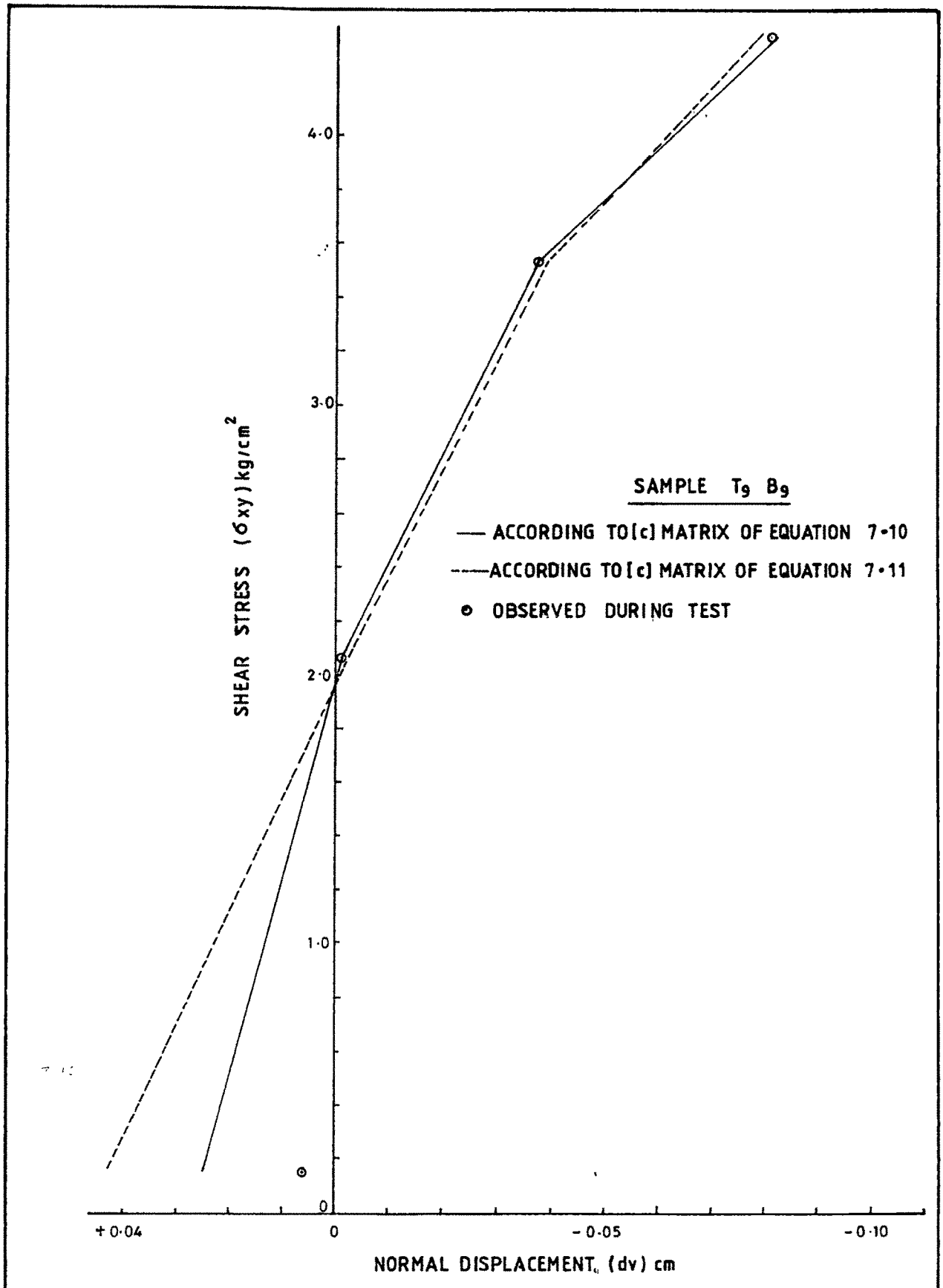

FIG: 7·10 COMPARISION OF OBSERVED AND PREDICTED DISPLACEMENTS -REGULARLY ASPIRATED SURFACE

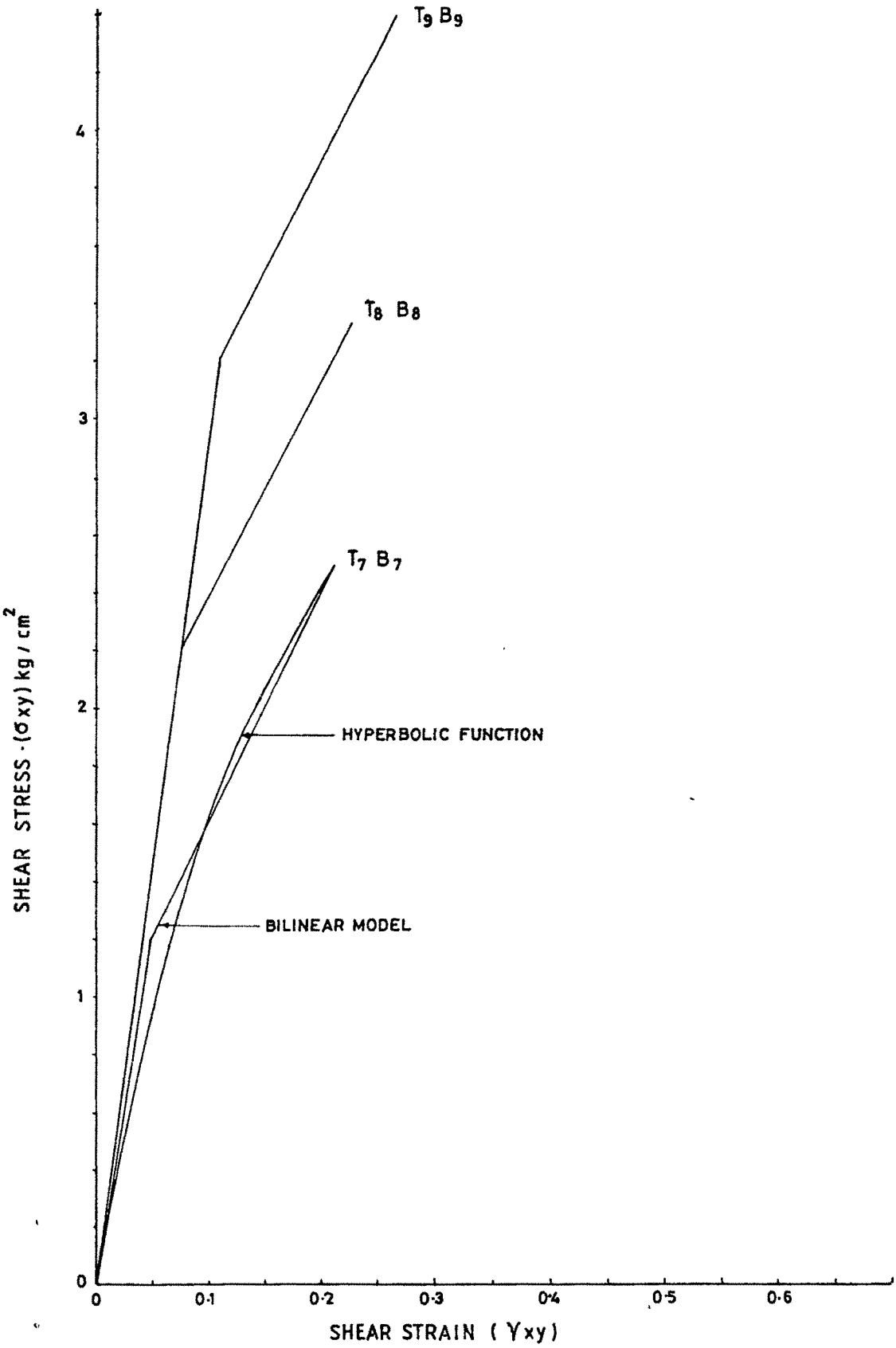

FIG: 7.11 RELATION BETWEEN SHEAR STRESS AND SHEAR STRAIN

-REGULARLY ASPIRATED SURFACES

$$\sigma_{xyc} = 1{\cdot}2\ (\sigma_{yy})^{1{\cdot}4} \qquad (7.14)$$

It is possible to model the above behaviour by a hyperbolic function,

$$\sigma_{xy} = \frac{y}{b + a\varepsilon_{xy}} \qquad (7.15)$$

Where, $\frac{1}{b}$ is the initial shear modulus equal to 25 so that b = 0.04 and 'a' will be different for different normal stresses.

7.5.2 The developed constitutive relationships are applied to test data of laboratory direct shear tests generated by Dave (1987), as reported in para 6.4. Table 7.8 exhibits normal and shear displacements observed during some of these tests. The displacements predicted by the developed constitutive relations are also shown. The observed and predicted displacements are plotted against shear stress in Fig. 7.12 to 7.16. It is evident that the constitutive relationships for the new joint element are efficient in reasonably predicting displacements for tests conducted by other research workers. It is also evident that constitutive relationship containing dilation parameter $D = \frac{i_{av}}{i_o}$ as given by equation 7.11 is more efficient in predicting the displacements.

7.5.3 Similar attempt is made to apply the constitutive relationships for the new joint element to the test data of cyclic direct shear tests, generated by Shah (1987) as reported in para 6.5. Normal and shear displacements observed during a few typical loading cycles of these tests are tabulated in Table 7.9. The predicted displacements using constitutive relationships developed are also shown in this table. The same are plotted versus shear stress in Fig. 7.17 to 7.19. It is seen that there is reasonable correlation between the observed and the predicted displacements.

TABLE 7.8 : COMPARISION OF OBSERVED AND PREDICTED DISPLACEMENTS FOR DATA OF LABORATORY DIRECT SHEAR TESTS CONDUCTED BY DAVE (1987)

Test Sample No.	Normal stress σ_{yy} kg/cm^2	Shear stress σ_{xy} kg/cm^2	Shear modulus 'G' kg/cm^2	Poisson's ratio 'ν'	Young's modulus 'E' kg/cm^2	Observed displacements		Predicted displacements as per equation 7.10		Predicted displacements as per equation 7.11	
						Normal dv cm	Shear du cm	Normal dv cm	Shear du cm	Normal dv cm	Shear du cm
A_2	23.42	10.09	250	1.02	1000	-0.004	0.400	-0.011	0.400	-0.005	0.400
	23.42	16.06	350	1.05	1500	-0.010	0.450	-0.020	0.440	-0.010	0.440
	23.42	21.52	414	1.05	1500	-0.013	0.525	-0.023	0.520	-0.010	0.520
A_6	74.79	14.56	650	0.99	2500	+0.001	0.225	+0.007	0.225	+0.003	0.225
	74.79	41.72	800	1.04	3200	-0.010	0.525	-0.023	0.525	-0.010	0.525
	74.79	46.85	700	1.06	2900	-0.021	0.675	-0.039	0.675	-0.019	0.675
	74.79	53.64	440	1.04	1800	-0.026	1.225	-0.046	1.225	-0.020	1.225
A_8	96.04	52.81	5280	1.10	22000	-0.005	0.100	-0.011	0.100	-0.005	0.100
	96.04	63.90	3651	1.09	15000	-0.007	0.175	-0.016	0.178	-0.007	0.178
	96.04	71.18	1900	1.06	7800	-0.010	0.375	-0.020	0.376	-0.009	0.376
	96.04	72.84	834	1.04	3400	-0.015	0.875	-0.031	0.874	-0.014	0.874
B_6	65.28	28.53	1700	1.10	7200	-0.007	0.150	-0.023	0.160	-0.012	0.160
	65.28	33.31	1400	1.13	6300	-0.014	0.225	-0.036	0.226	-0.017	0.226
	65.28	36.05	1100	1.14	4700	-0.021	0.325	-0.050	0.320	-0.025	0.320
D_1	9.27	1.96	78	1.36	370	-0.039	0.250	-0.100	0.250	-0.050	0.250
	9.27	4.91	140	1.34	700	-0.053	0.350	-0.125	0.320	-0.066	0.320
	9.27	6.06	121	1.27	550	-0.063	0.500	-0.130	0.500	-0.060	0.500
C_2	21.09	11.75	224	1.02	905	-0.004	0.525	-0.012	0.524	-0.005	0.524
	21.09	12.25	196	1.03	800	-0.010	0.625	-0.020	0.620	-0.010	0.620
	21.09	12.41	177	1.04	723	-0.013	0.700	-0.030	0.700	-0.014	0.700

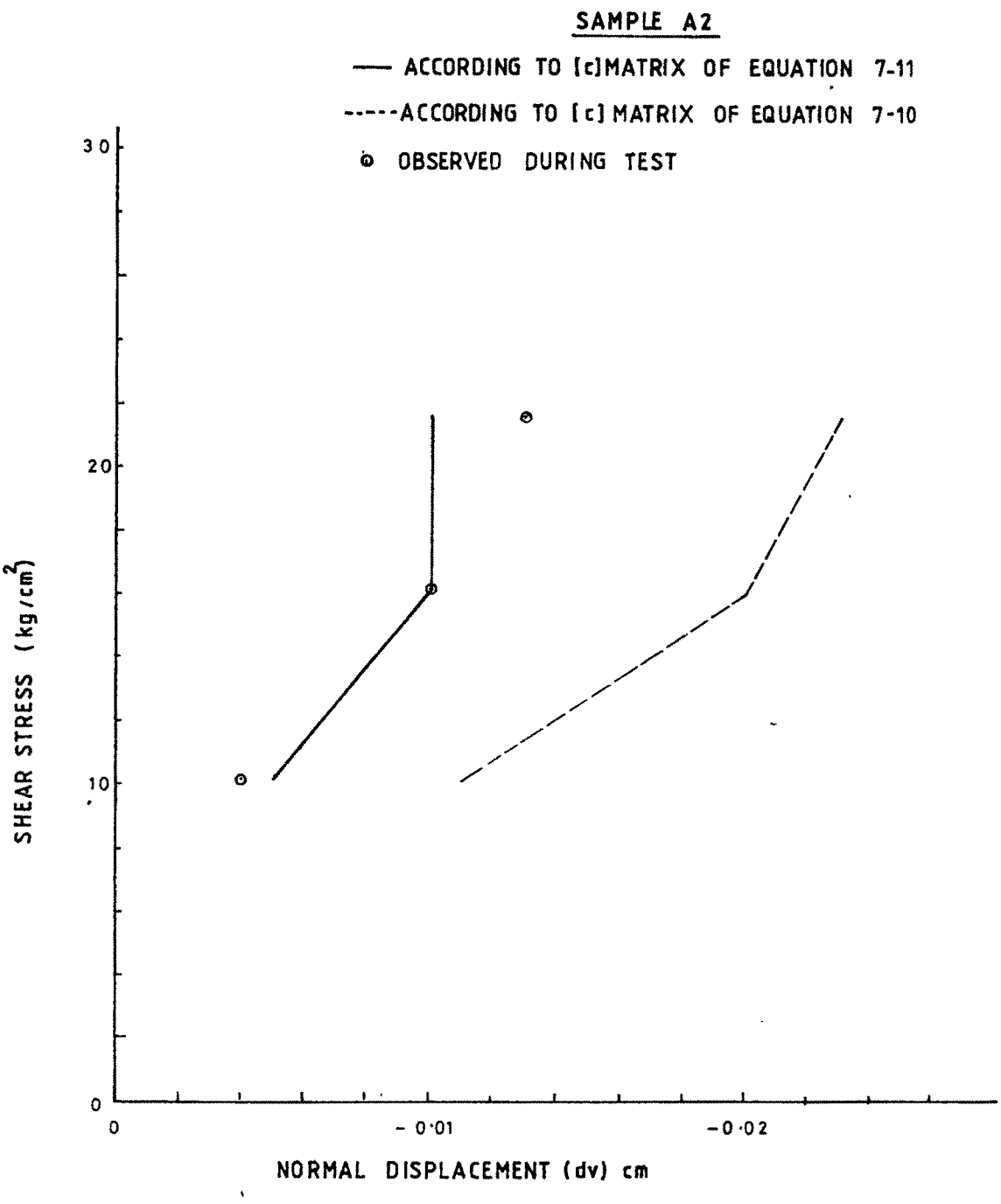

FIG: 7·12 COMPARISION OF OBSERVED AND PREDICTED DISPLACEMENTS

-DAVE (1987)

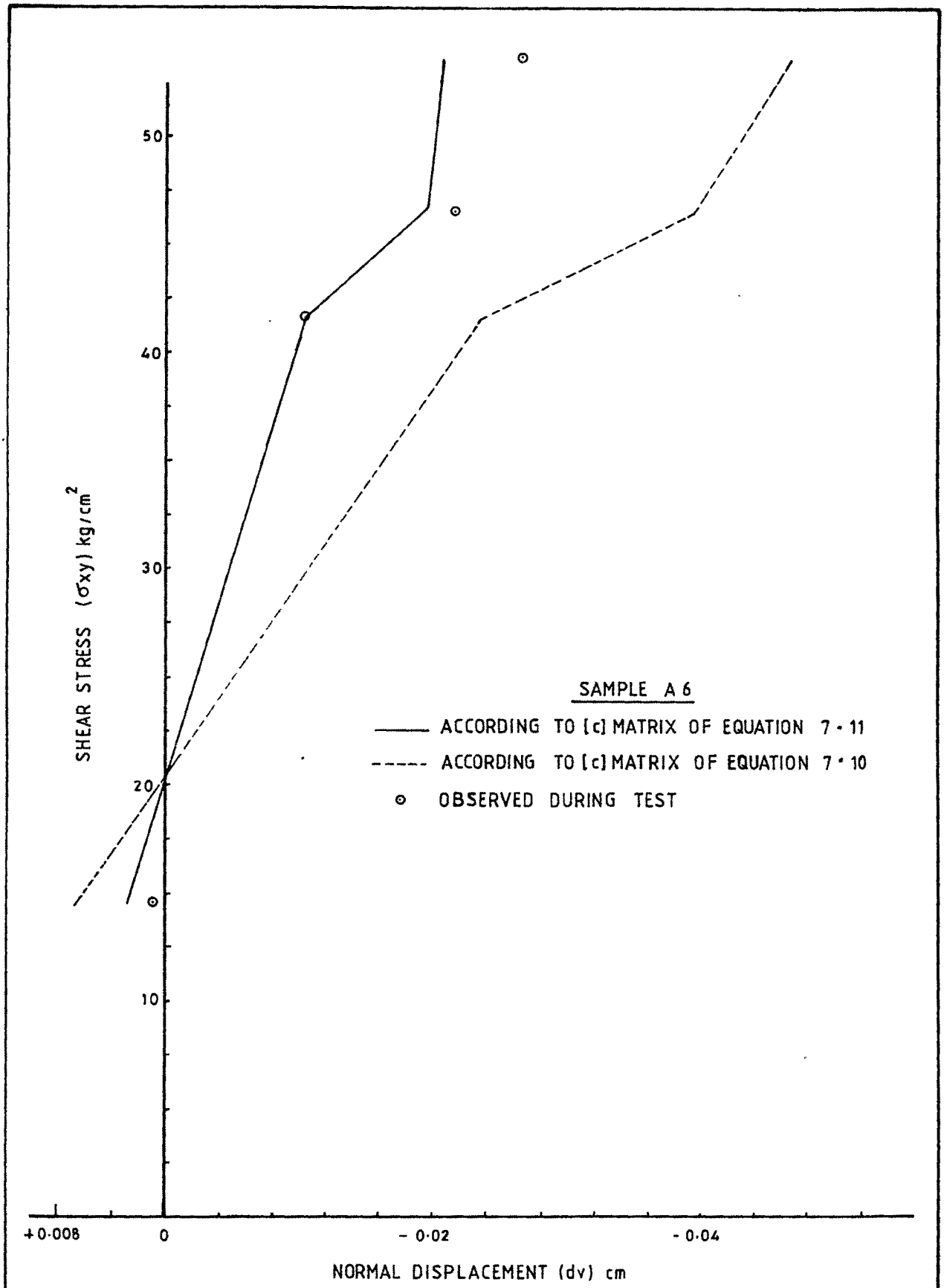

FIG: 7·13 COMPARISION OF OBSERVED AND PREDICTED DISPLACEMENTS

DAVE (1987)

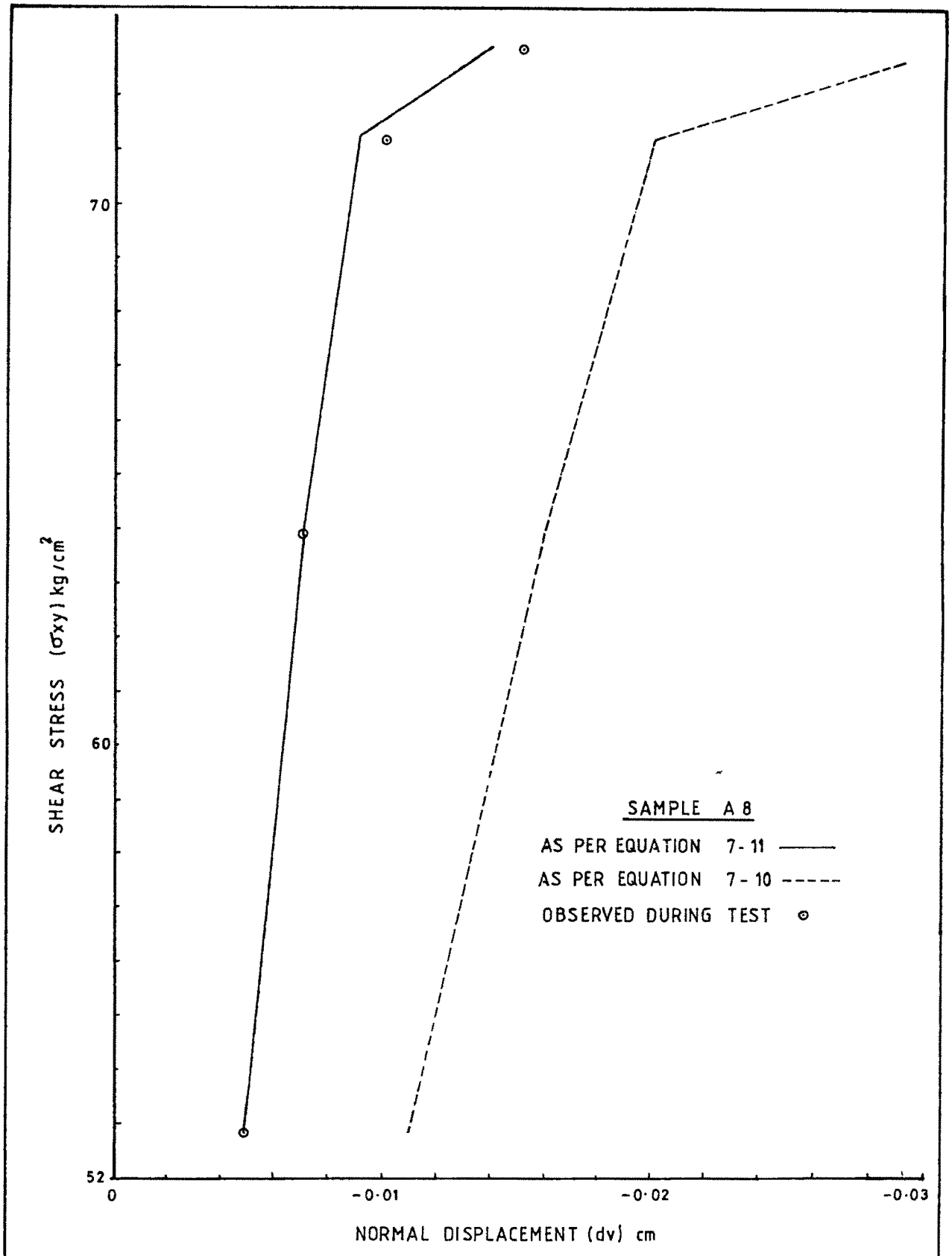

FIG: 7.14 COMPARISION OF OBSERVED AND PREDICTED DISPLACEMENTS

DAVE (1987)

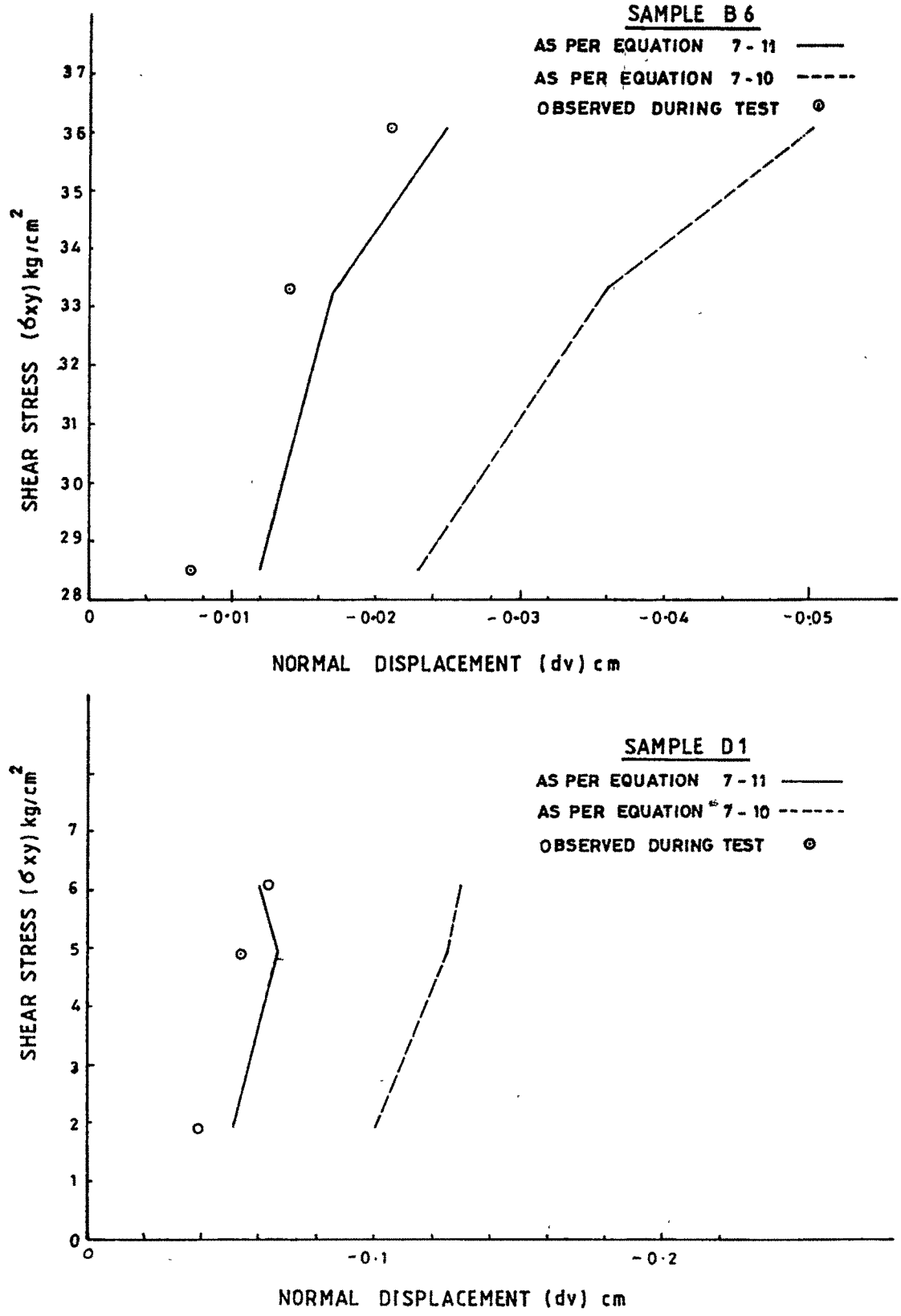

FIG: 7.15 COMPARISION OF OBSERVED AND PREDICTED DISPLACEMENTS

- DAVE (1987)

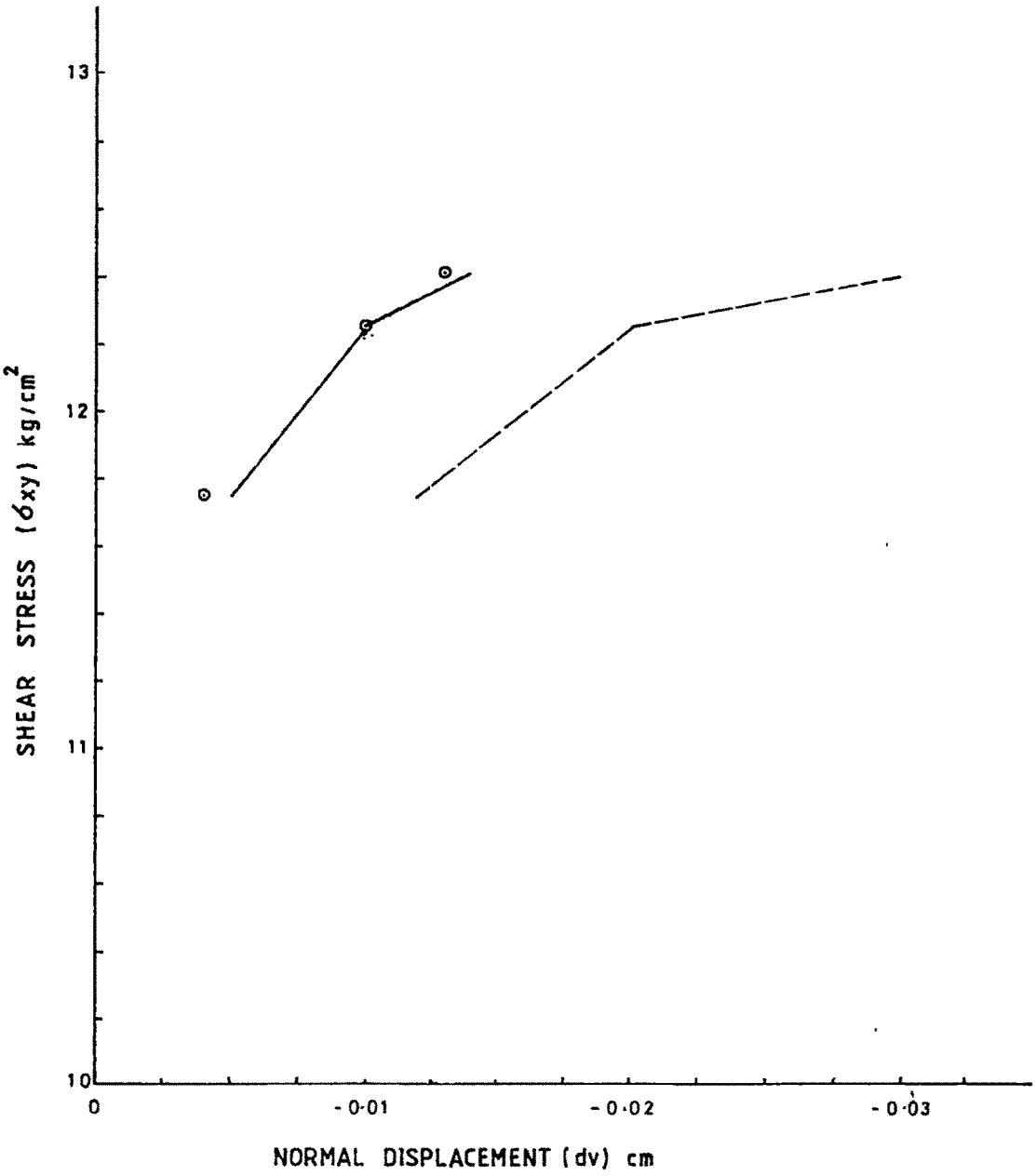

FIG: 7·16 COMPARISION OF OBSERVED AND PREDICTED DISPLACEMENTS

- DAVE (1987)

TABLE 7.9 : COMPARISION OF OBSERVED AND PREDICTED DISPLACEMENTS FOR DATA OF CYCLIC DIRECT SHEAR TESTS CONDUCTED BY SHAH (1987)

Test Sample No.	Normal stress σ_{yy} kg/cm^2	Shear stress σ_{xy} kg/cm^2	Shear modulus 'G' kg/cm^2	Poisson's ratio 'ν'	Young's modulus 'E' kg/cm^2	Observed displacements		Predicted displacements as per equation 7.10		Predicted displacements as per equation 7.11	
						Normal dv cm	Shear du cm	Normal dv cm	Shear du cm	Normal dv cm	Shear du cm
A_2 F(III)	20.87	3.28	328	1.00	1300	0.000	0.100	0.000	0.100	0.000	0.100
	20.87	3.44	312	1.04	1276	-0.002	0.110	-0.014	0.110	-0.003	0.110
	20.87	3.93	302	1.08	1260	-0.005	0.130	-0.030	0.130	-0.006	0.130
	20.87	3.93	280	1.09	1170	-0.006	0.140	-0.033	0.140	-0.008	0.140
A_6 F(V)	62.63	23.44	1562	1.00	6250	0.000	0.150	0.000	0.150	0.000	0.150
	62.63	23.60	1388	1.01	5580	-0.001	0.170	-0.002	0.170	-0.0005	0.170
	62.63	23.93	1087	1.03	4416	-0.003	0.220	-0.010	0.220	-0.002	0.220
	62.63	24.10	588	1.02	2375	-0.005	0.410	-0.010	0.410	-0.003	0.410
C_4 F(IV)	41.50	21.30	790	1.00	3150	0.000	0.270	0.000	0.270	0.000	0.270
	41.50	22.12	630	1.01	2540	-0.002	0.350	-0.004	0.350	-0.0008	0.350
	41.50	22.29	582	1.02	2350	-0.004	0.400	-0.009	0.400	-0.0017	0.400
	41.50	22.45	430	1.04	1760	-0.011	0.520	-0.024	0.520	-0.004	0.520

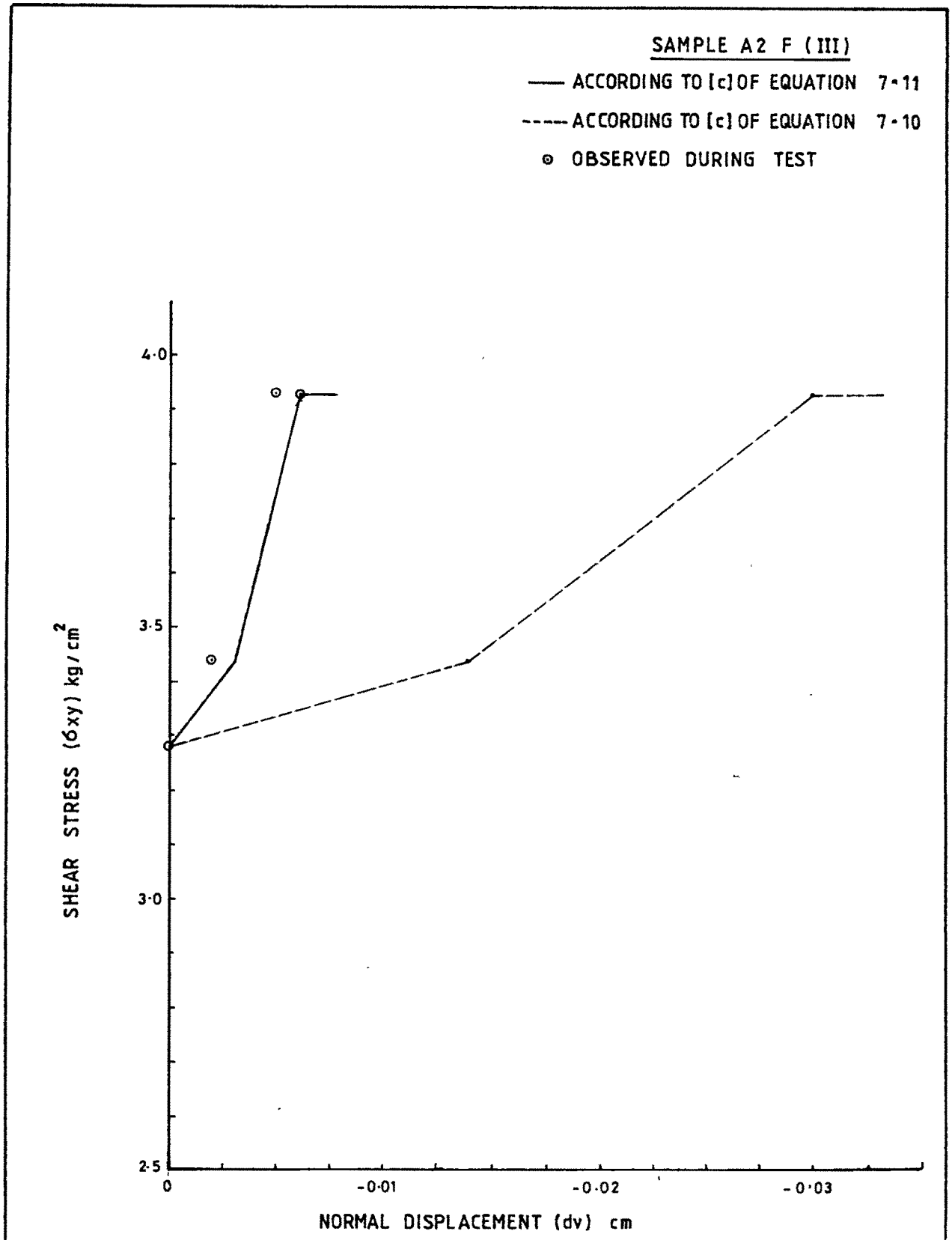

FIG: 7.17 COMPARISION OF OBSERVED AND PREDICTED DISPLACEMENTS

-SHAH (1987)

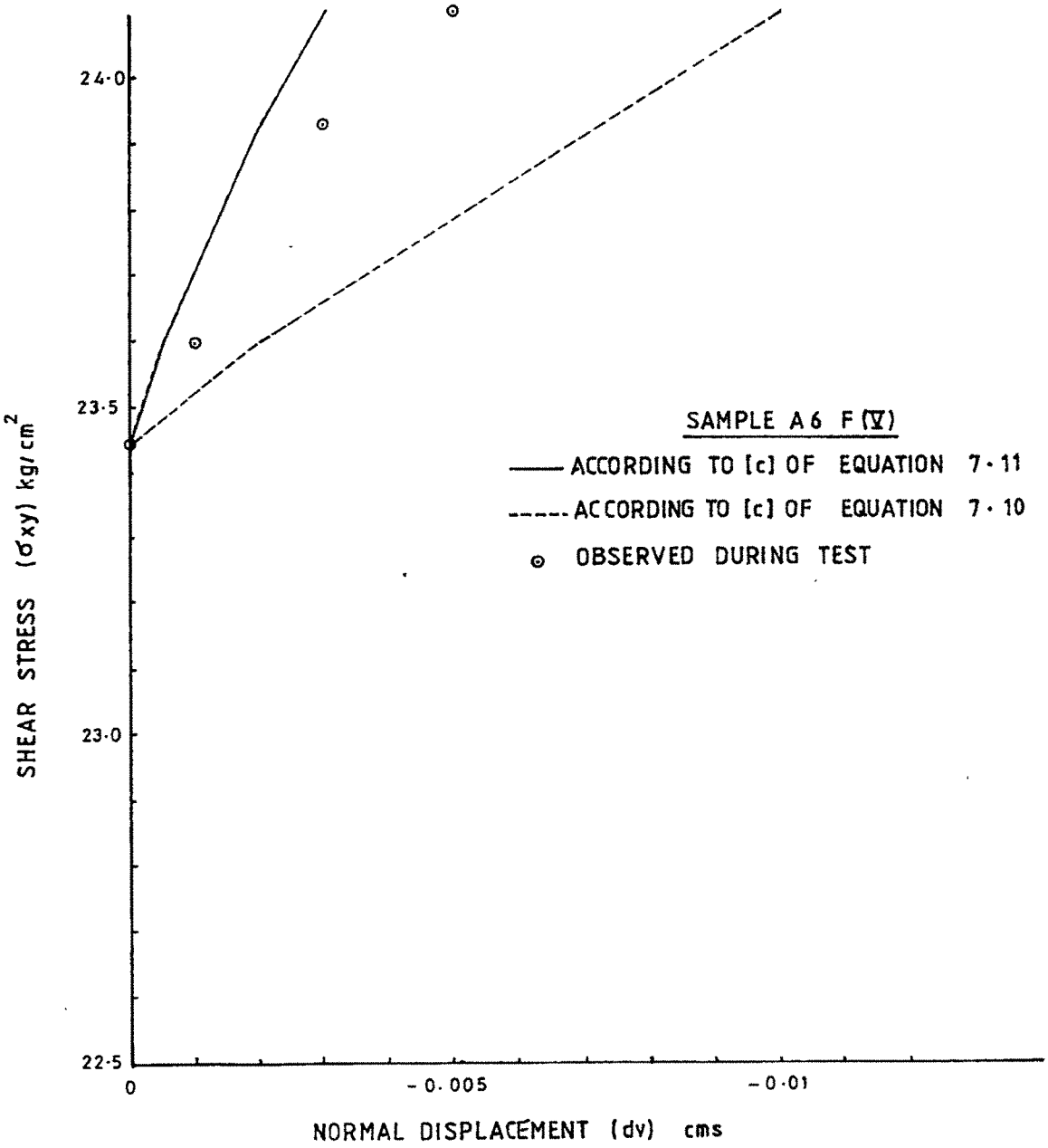

FIG: 7·18 COMPARISION OF OBSERVED AND PREDICTED DISPLACEMENTS

- SHAH (1987)

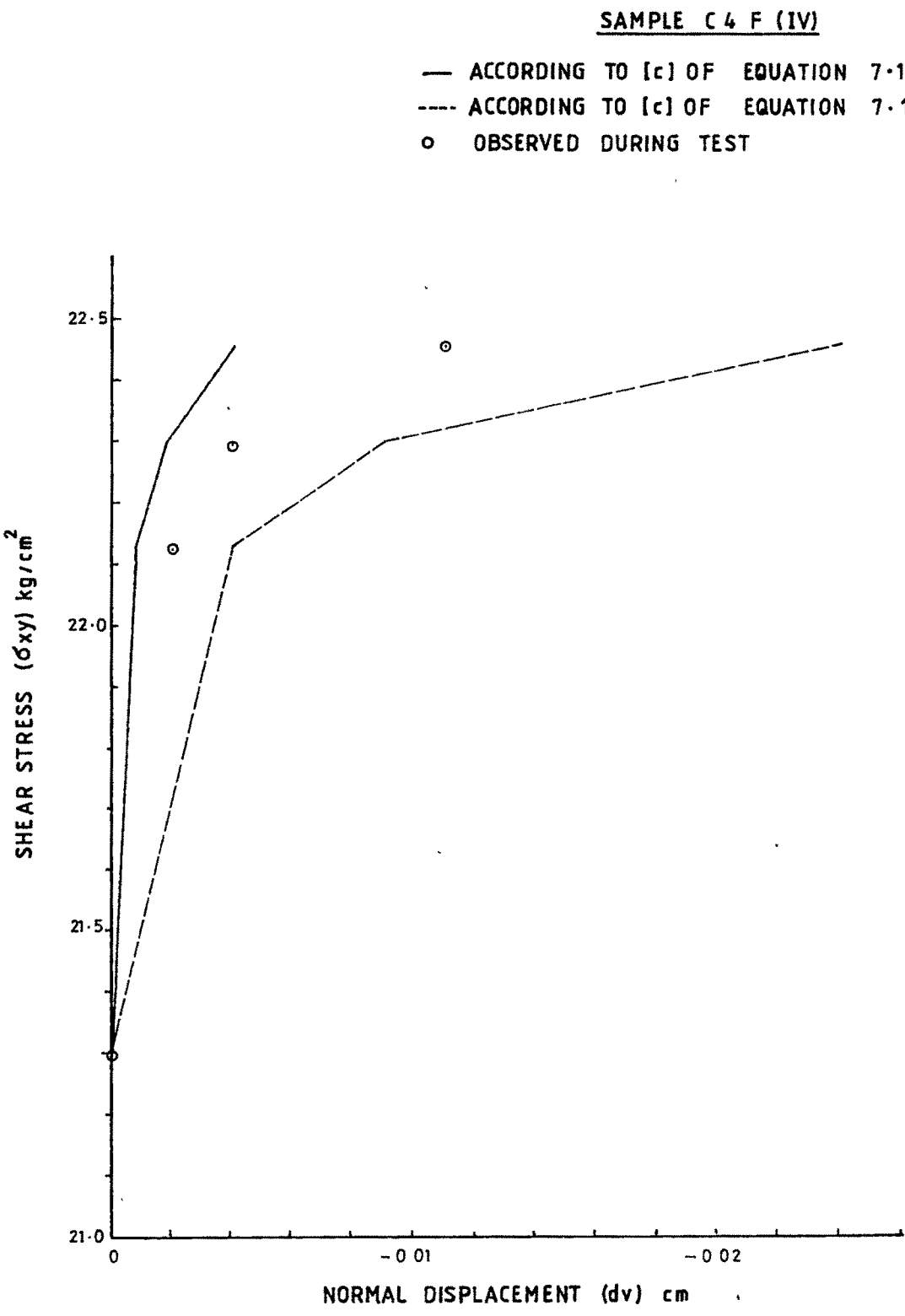

FIG: 7·19 COMPARISION OF OBSERVED AND PREDICTED DISPLACEMENT

- SHAH (1987)

7.5.4 The test data of insitu shear tests on concrete-rock interface generated by Datir' (1981) is already reported in para 6.6. The observed displacements during some of these tests are tabulated alongwith those predicted by the developed constitutive relations in Table 7.10. The observed and predicted normal displacements are also plotted in Fig. 7.20 to 7.25. The constitutive relationships have shown their efficiency in closely predicting the data of insitu tests. The constitutive relationship of equation 7.11 is found to be more efficient than the other one.

7.6 APPLICATIONS OF DEVELOPED JOINT ELEMENT

7.6.1 General

In order to verify the applicability of the developed constitutive matrices in the established finite element programmes, it is decided to incorporate the developed constitutive matrix of equation 7.11 in the 2D plane stress/plane strain isoparamatric element finite element programme developed by Owen and Hinton (1977). The programme listing is given in Appendix-II. The part of the programme incorporating constitutive matrix is modified to allow for the developed constitutive matrix of the joint element as given in equation 7.11 to be incorporated. The changes made are also shown in Appendix-II.

The programme utilises 8 nodel isoparamatric elements for the continuum. It is proposed to use similar elements for the joint elements also. Thus the joint elements are considered same as solid elements in geometry. Thickness of the joint elements will be appropriate to the problem under study. Thus joint elements will have some thickness like the thin element proposed by Desai (1984). The properties of joint elements such as Poisson's ratio and Young's Modulus are considered as variables.

TABLE 7.10 : COMPARISION OF OBSERVED AND PREDICTED DISPLACEMENTS FOR DATA OF IN SITU SHEAR TESTS REPORTED BY DATIR (1981)

Test Sample No.	Normal stress σ_{yy} kg/cm^2	Shear stress σ_{xy} kg/cm^2	Shear modulus 'G' kg/cm^2	Poisson's ratio 'ν'	Young's modulus 'E' kg/cm^2	Observed displacements		Predicted displacements as per equation 7.10		Predicted displacements as per equation 7.11	
						Normal dv cm	Shear du cm	Normal dv cm	Shear du cm	Normal dv cm	Shear du cm
1	6.76	10.34	17200	1.10	76000	-0.001	0.018	-0.001	0.017	-0.0007	0.017
	7.00	11.20	16000	1.22	71000	-0.002	0.020	-0.0024	0.020	-0.0018	0.020
	7.57	13.35	6675	1.47	33000	-0.011	0.060	-0.0138	0.060	-0.010	0.060
	7.80	14.21	2842	1.74	16000	-0.041	0.140	-0.048	0.140	-0.039	0.140
2	5.77	3.66	30500	1.31	140000	-0.0005	0.0035	-0.0011	0.0036	-0.001	0.0036
	6.81	7.54	25000	1.32	111000	-0.001	0.009	-0.0013	0.009	-0.0011	0.009
	8.02	12.06	8614	1.53	43600	-0.010	0.042	-0.012	0.042	-0.010	0.042
	8.14	12.49	3900	1.54	20000	-0.020	0.096	-0.027	0.095	-0.021	0.095
3(III)	10.91	9.82	7000	1.11	30000	-0.002	0.041	-0.0035	0.041	-0.0031	0.041
	12.15	14.22	5270	1.17	23000	-0.005	0.082	-0.009	0.080	-0.007	0.080
	13.07	17.94	1200	1.14	5100	-0.030	0.450	-0.038	0.450	-0.028	0.450
	13.55	19.67	855	1.30	4000	-0.086	0.687	-0.078	0.680	-0.087	0.680
4	9.00	11.20	28000	1.03	113680	-0.0002	0.012	-0.0005	0.012	-0.0003	0.012
	9.23	12.06	14000	1.59	73000	-0.006	0.026	-0.008	0.026	-0.007	0.026
	9.42	12.43	11300	1.43	55000	-0.007	0.033	-0.008	0.033	-0.007	0.033
	9.80	14.23	6468	1.57	33000	-0.016	0.067	-0.018	0.066	-0.017	0.066
5(III)	18.83	27.05	38643	1.22	172000	-0.002	0.023	-0.0024	0.020	-0.002	0.020
	19.87	30.88	28072	1.71	152000	0.008	0.034	-0.012	0.033	-0.010	0.033
	20.90	34.74	26723	1.75	147000	-0.013	0.046	-0.014	0.039	-0.012	0.039
5(IV)	6.17	7.72	19300	1.42	93000	0.002	0.0125	-0.003	0.012	-0.002	0.012
	8.24	15.44	15440	1.81	86800	-0.010	0.029	-0.01	0.030	-0.007	0.030
	10.31	23.16	8000	2.70	59100	-0.045	0.086	-0.102	0.086	-0.090	0.086

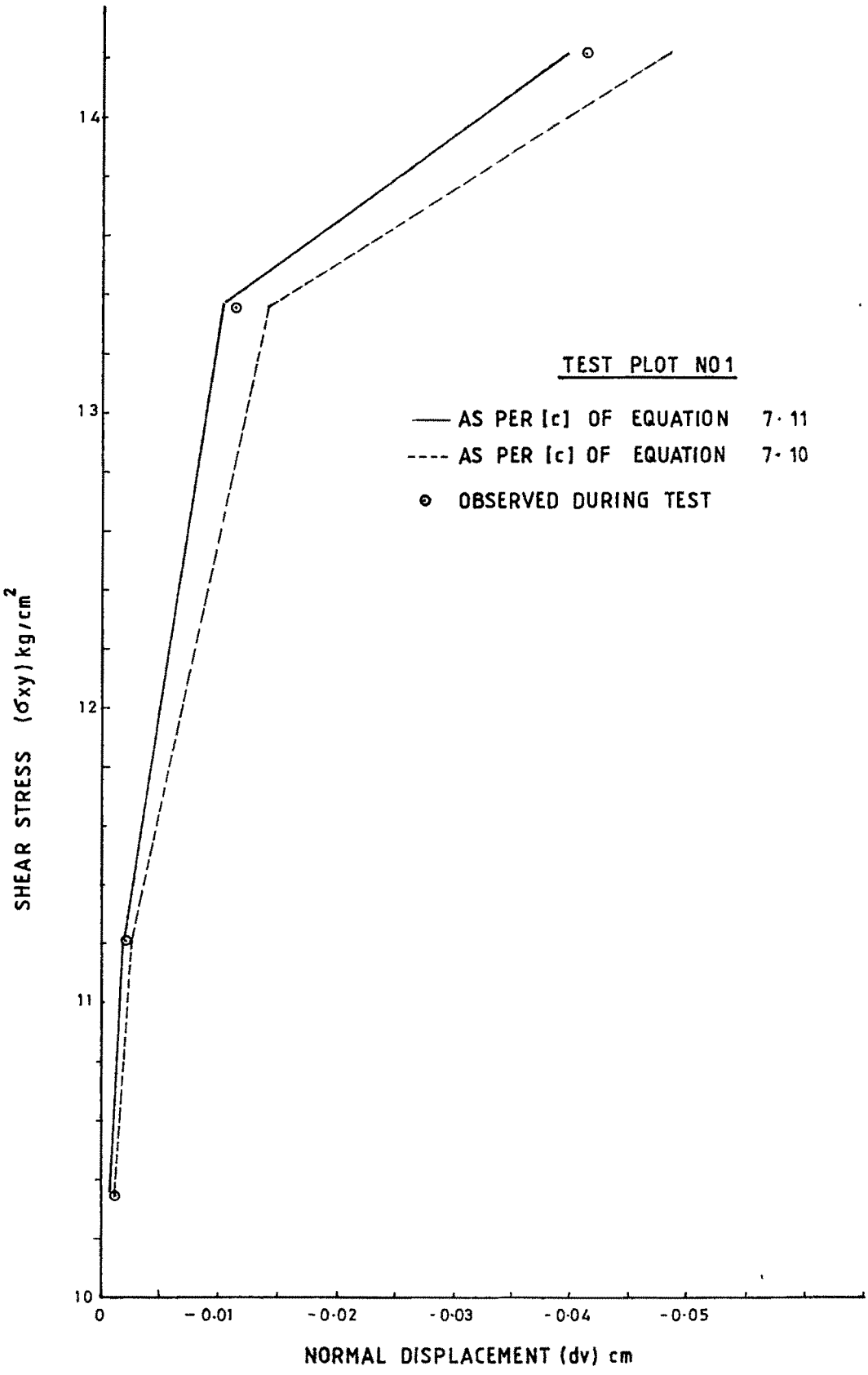

FIG: 7·20 COMPARISION OF OBSERVED AND PREDICTED DISPLACEMENTS

- DATIR (1981)

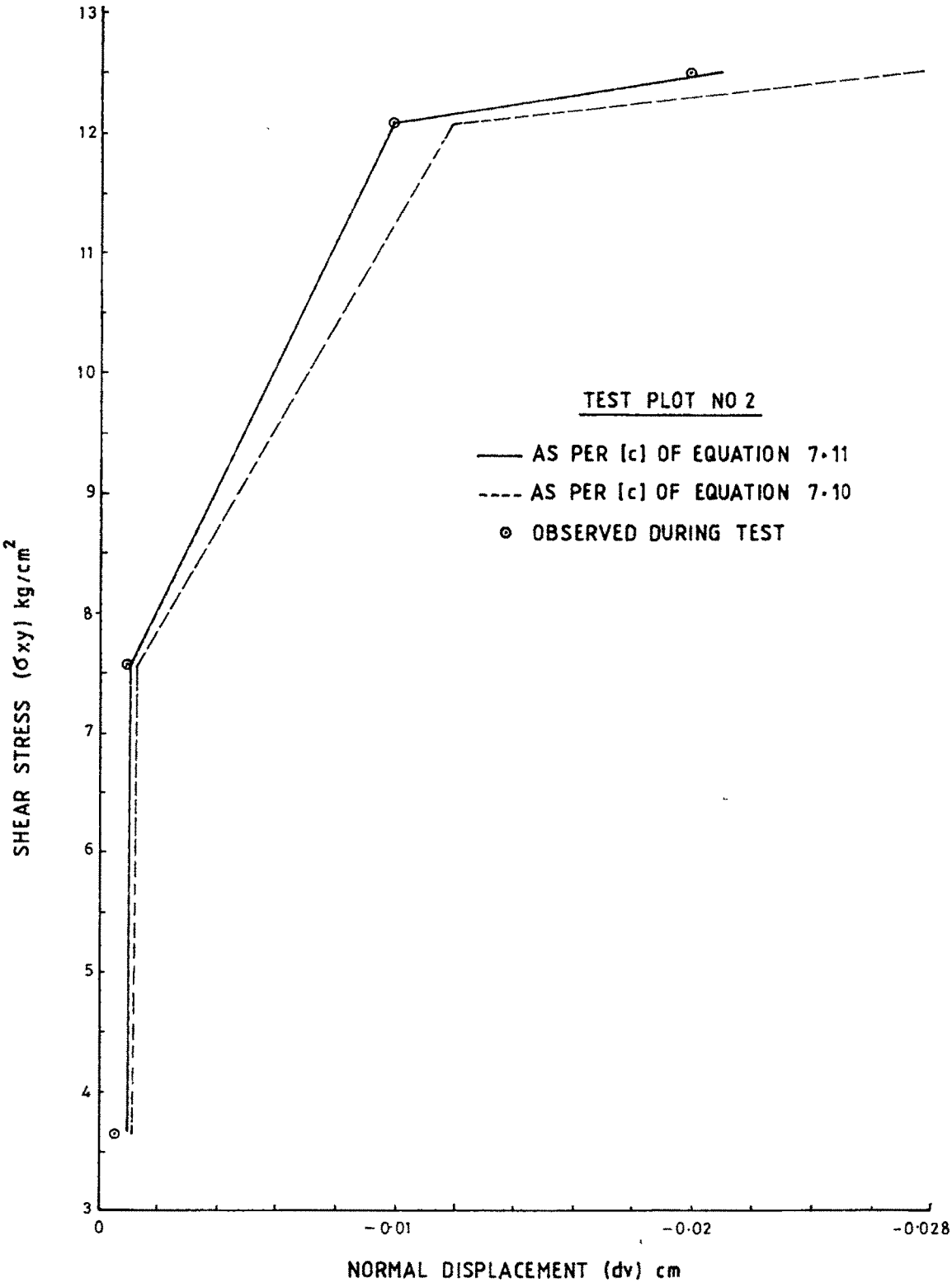

FIG: 7·21 COMPARISION OF OBSERVED AND PREDICTED DISPLACEMENTS

-DATIR (1981)

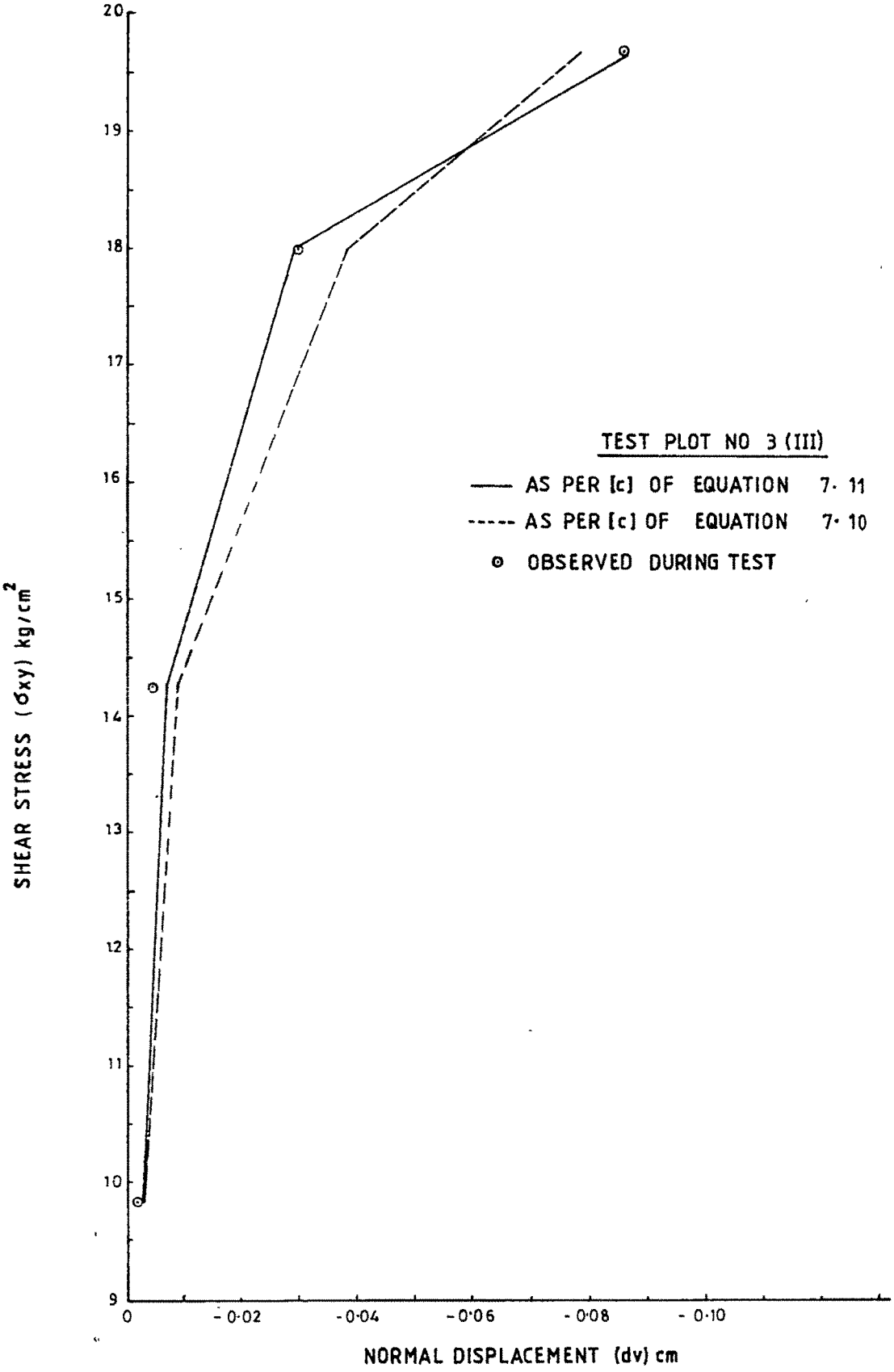

FIG:7·22 COMPARISION OF OBSERVED AND PREDICTED DISPLACEMENTS

-DATIR (1981)

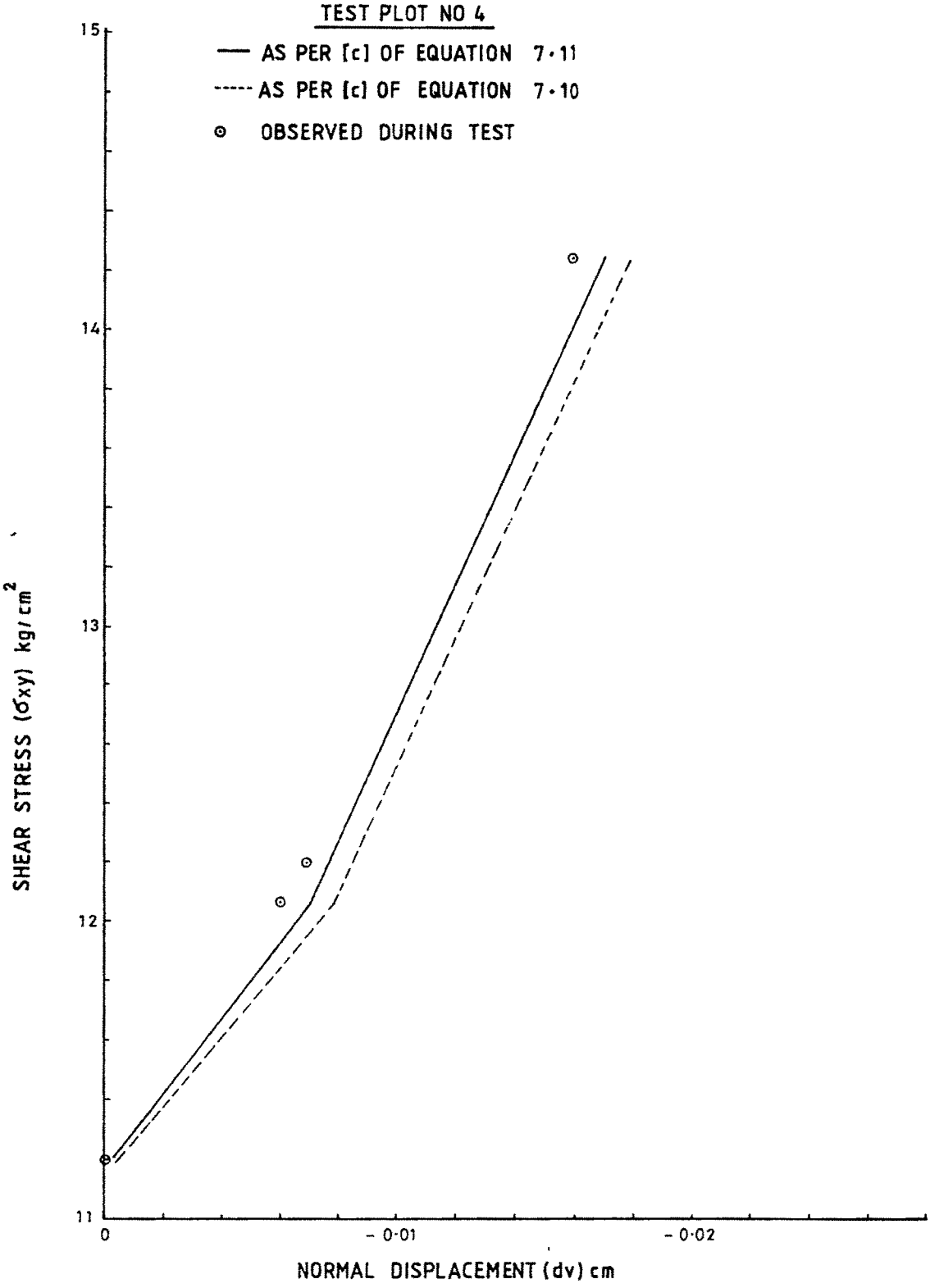

FIG:7·23 COMPARISION OF OBSERVED AND PREDICTED DISPLACEMENTS

-DATIR (1981)

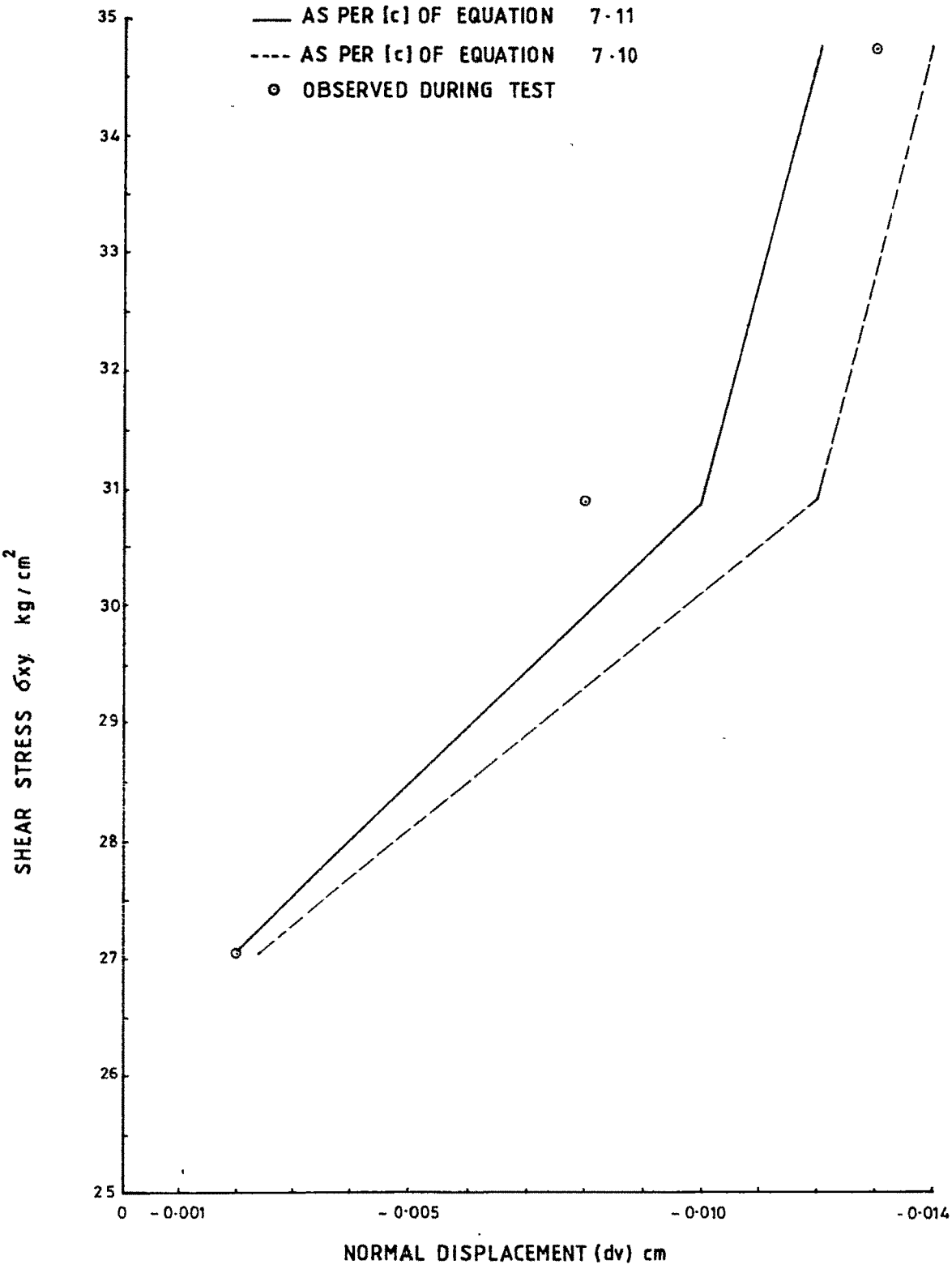

FIG: 7·24 COMPARISION OF OBSERVED AND PREDICTED DISPLACEMENTS

-DATIR (1981)

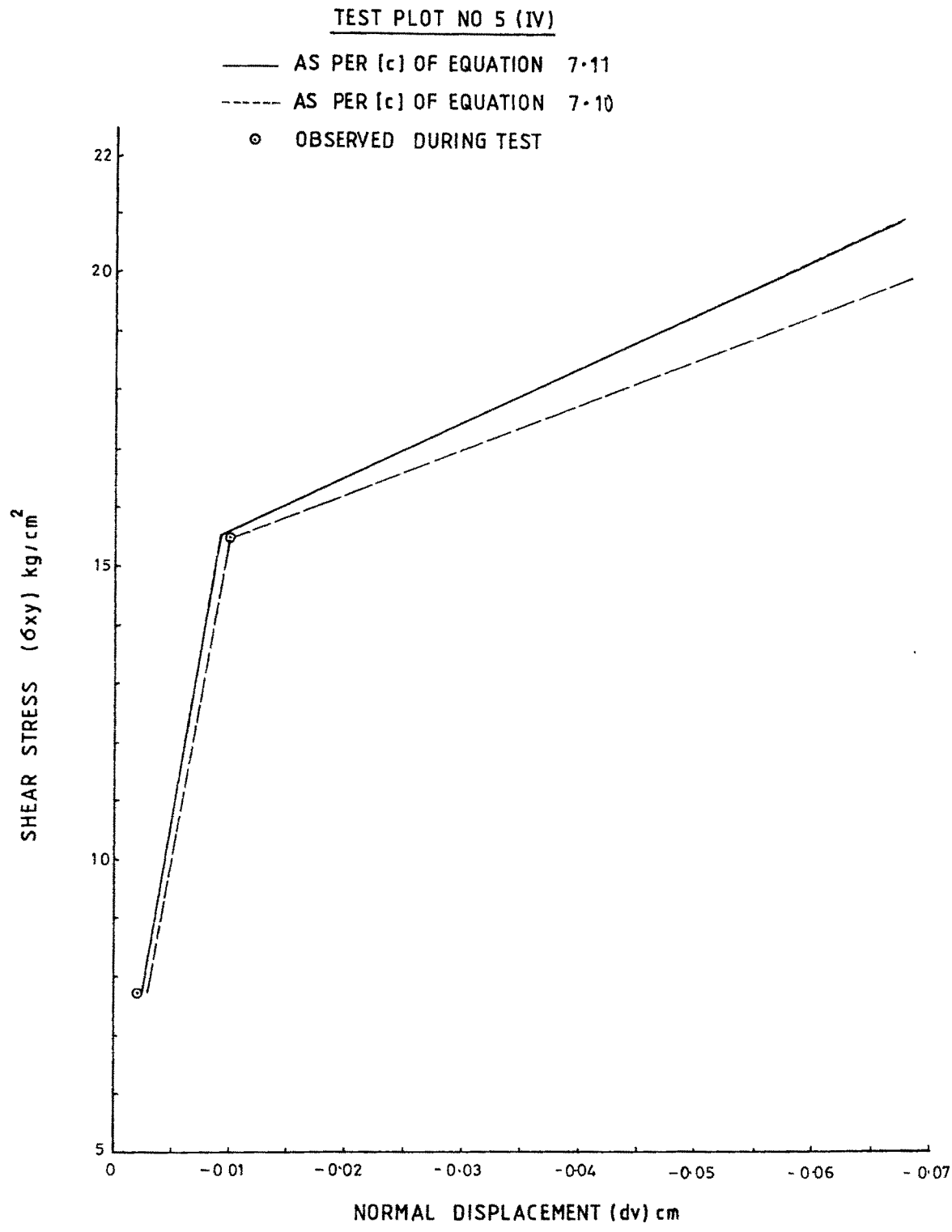

FIG: 7·25 COMPARISION OF OBSERVED AND PREDICTED DISPLACEMENTS

-DATIR (1981)

It is proposed to apply this finite element programme to following cases :

(i) Laboratory direct shear tests conducted on regularly aspereted samples.

(ii) Laboratory direct shear tests conducted and reported by Dave (1987).

(iii) Laboratory cyclic direct shear tests conducted and reported by Shah (1987).

(iv) In situ direct shear tests conducted by Datir (1981).

(v) Single joint element discussed by Desai et al (1984).

(vi) Two dimensional case discussed by Desai et al (1984).

(vii) Case of a thick circular cylinder, typical of a tunnel in a jointed rock, discussed by Hinton and Owen (1977).

The details of these applications with results obtained are discussed in the following paras.

7.6.2 Laboratory Tests conducted on Aspereted Samples

Regularly aspereted sample tested in laboratory is discretized as shown in Fig. 7.26. Shear stress - shear strain curves of these samples are shown in Fig. 7.27 to 7.29. From these curves values of G at various stages of shear load are evaluated by drawing radial lines from origin. From such value of G and corresponding value of ν shown in Table 7.4 to 7.6, value

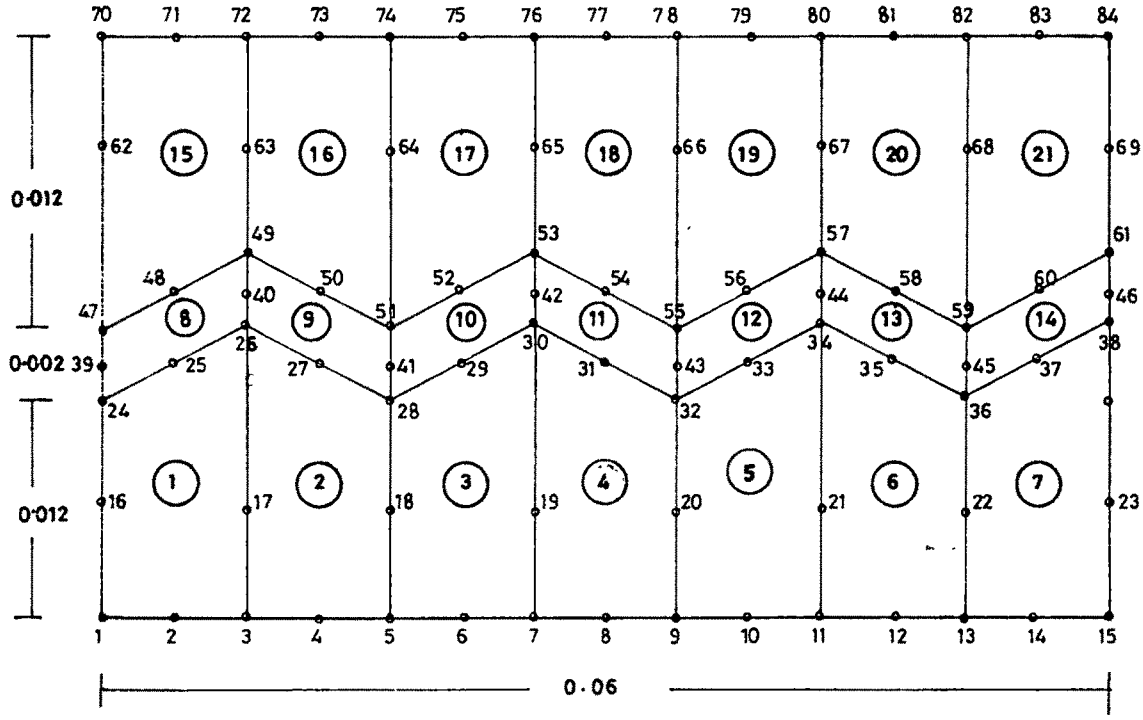

FIG: 7·26 DISCRETIZATION OF REGULARLY ASPIRATED SAMPLE TESTED IN DIRECT SHEAR BOX

REGULARLY ASPIRATED SAMPLE T_7 B_7

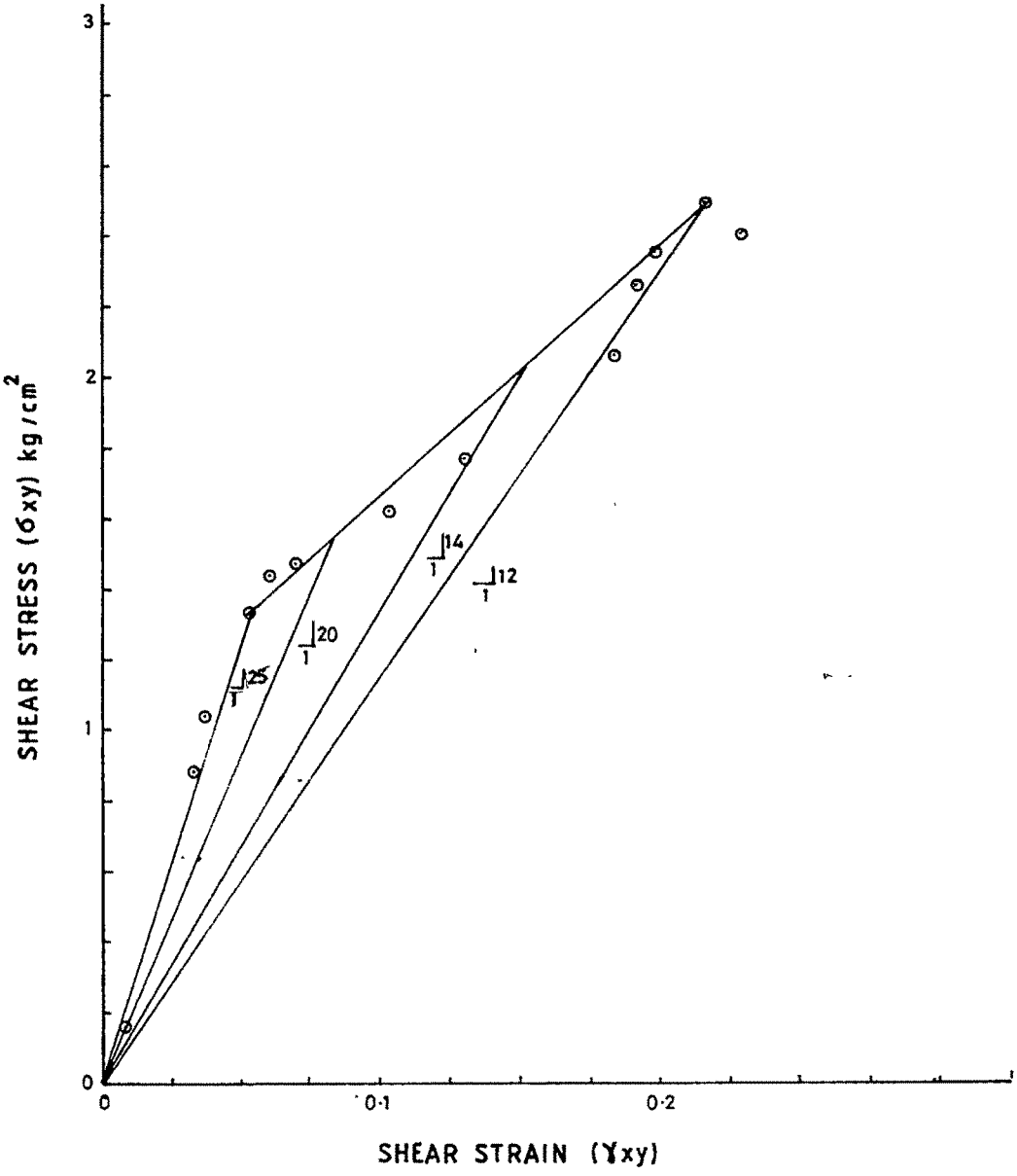

FIG: 7·27 SHEAR STRESS - SHEAR STRAIN RELATIONSHIP

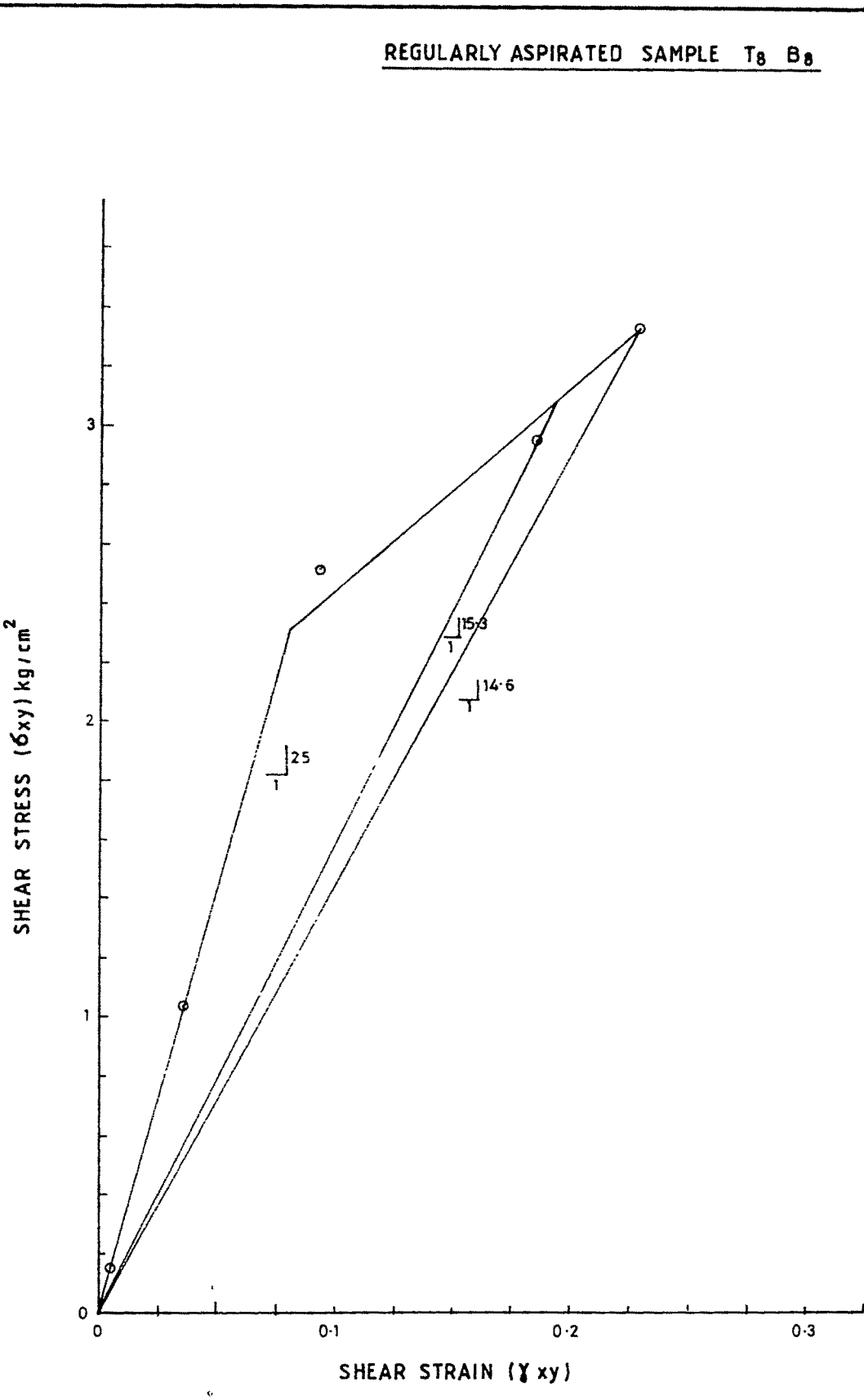

FIG: 7·28 SHEAR STRESS - SHEAR STRAIN RELATIONSHIP

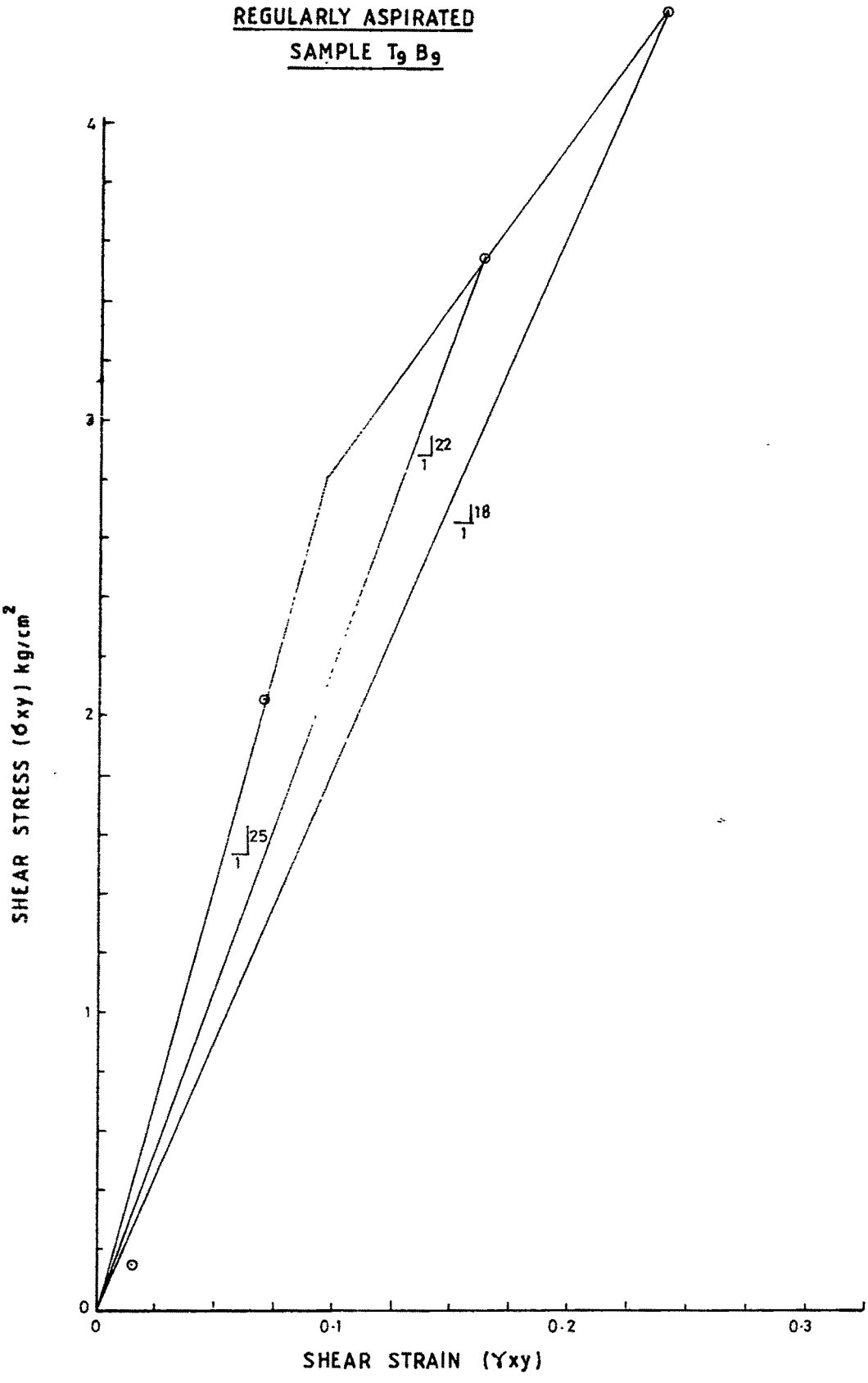

FIG: 7.29 SHEAR STRESS-SHEAR STRAIN RELATIONSHIP

of E is worked out. These values of E and ν are fed in the computer input data for the joint elements. Appropriate values of these material properties are selected for other material elements. Observed and computed values of normal displacement at various stages of shear load are presented in Fig. 7.30 to 7.32. It is evident that the developed joint element has remained successful in estimating accurately the observed normal displacements for all the tests.

7.6.3 Laboratory Tests conducted by Dave (1987)

Sample tested by Dave (1987) is discretized as shown in Fig. 7.33. For simplicity the sample has been discretized in only three elements. An average asperity angle is estimated to be 15°. Therefore, a geometrical asperity of this value is introduced in the joint element. Values of G, ν and E for the joint element are selected in the similar manner as discussed under para 7.6.2. The observed and computed values of normal displacements are presented in Fig. 7.34 to 7.36. The general observed trend of variation of normal displacement has been followed by the computed values, although the numerical values are differing. The difference between observed and computed values is attributed to variation in the size of the sample. Sample tested was 10cm x 10cm x 10 cm whereas the size of the element selected was 15cm x 15cm x 15cm, for convenience. Therefore, the load/unit area has reduced and hence the computed values of displacements appear to be on lower side. The other reason could be the fact that the sample is discretized in only three elements for simplicity.

7.6.4 Cyclic Direct Shear Tests conducted by Shah (1987)

Sample tested by Shah (1987) was similar to that tested by Dave (1987), which is discretized as shown in Fig. 7.33. The only difference is that the geometrical asperity of 20° is introduced in place of 15°. The observed and computed values of normal displacements for a few loading cycles are shown in Fig. 7.37 and

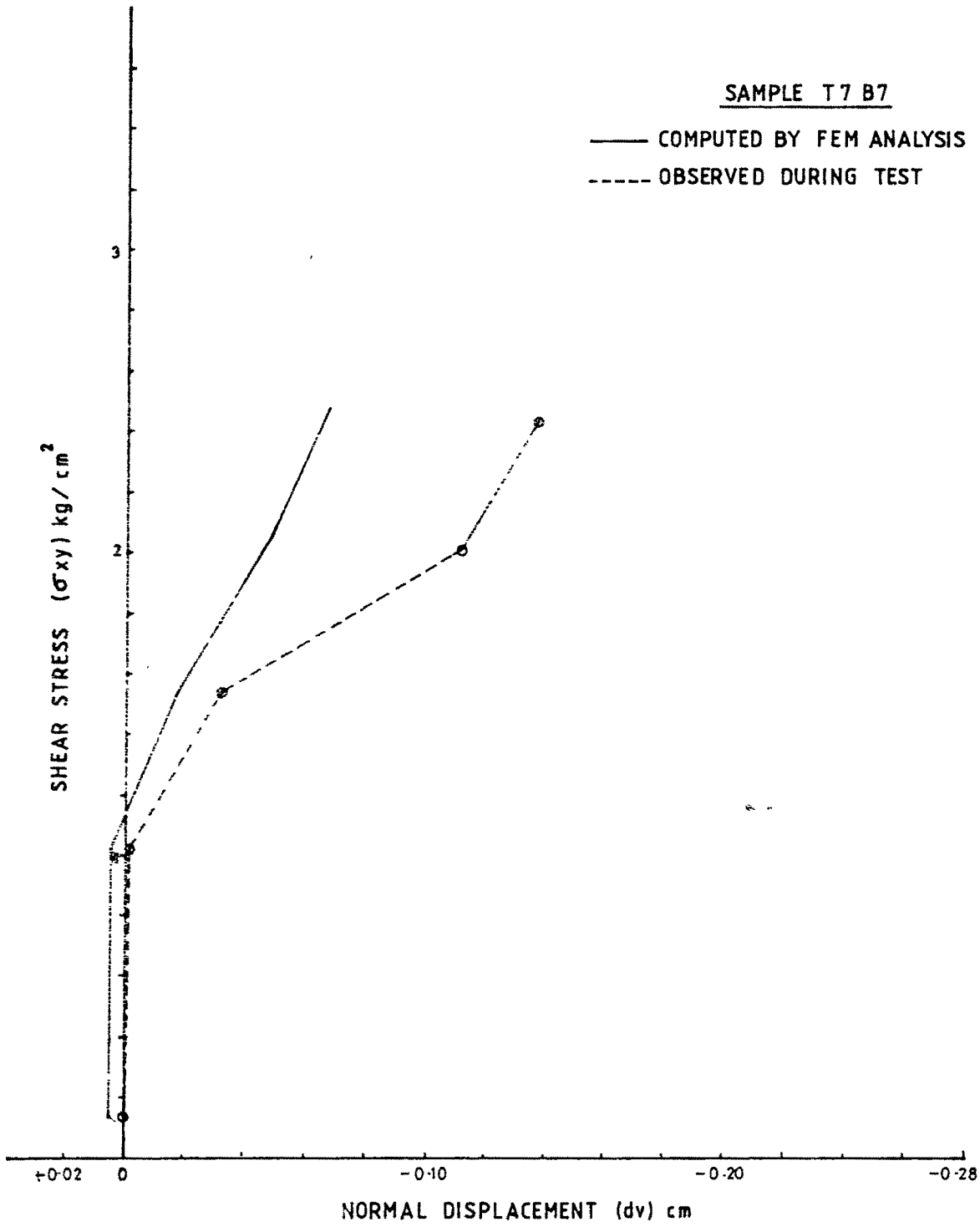

FIG:7-30 COMPARISION OF COMPUTED AND OBSERVED DISPLACEMENTS

-REGULARY ASPIRATED SURFACES

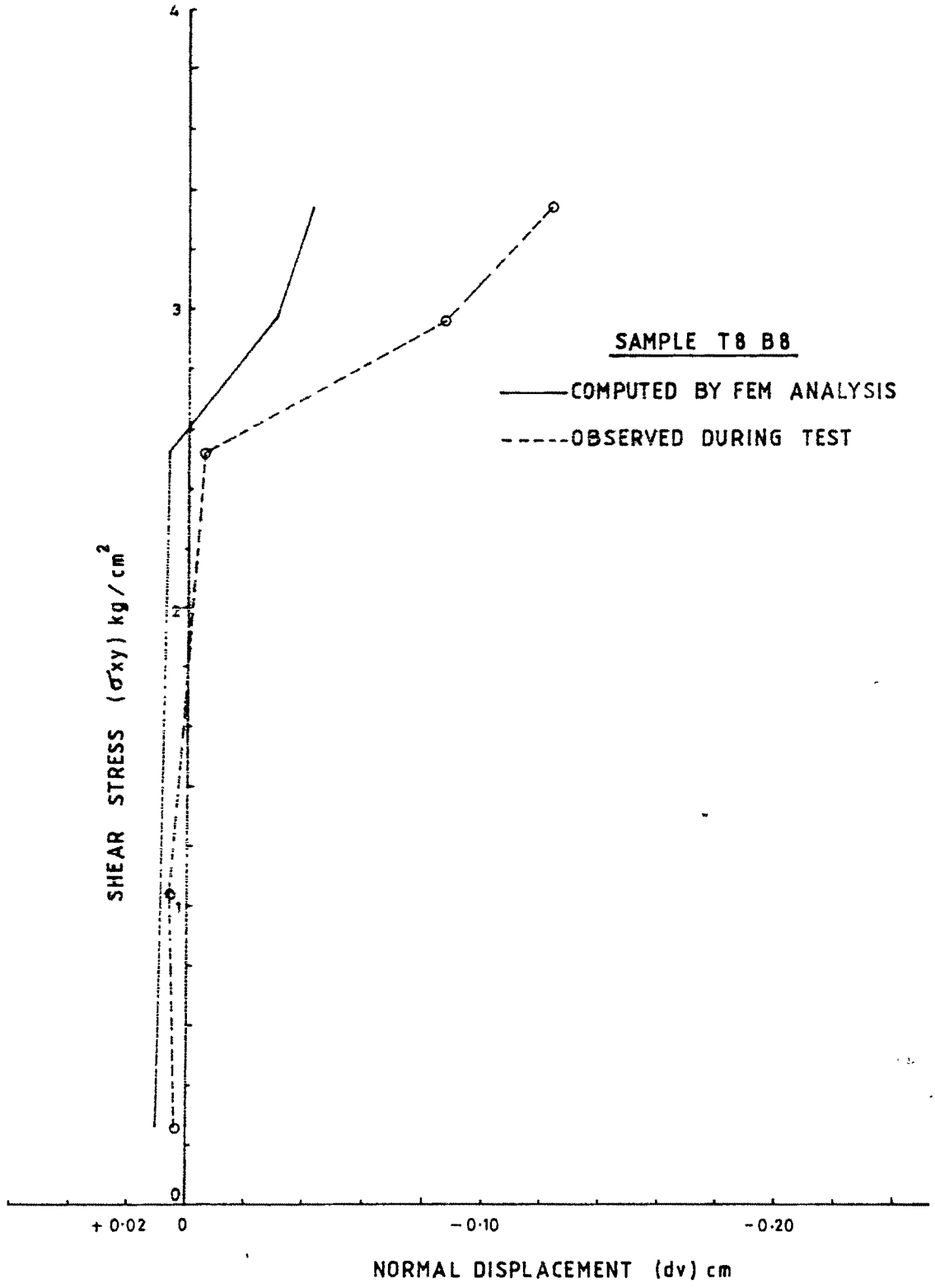

FIG: 7·31 COMPARISION OF COMPUTED AND OBSERVED DISPLACEMENTS

-REGULARLY ASPIRATED SURFACES

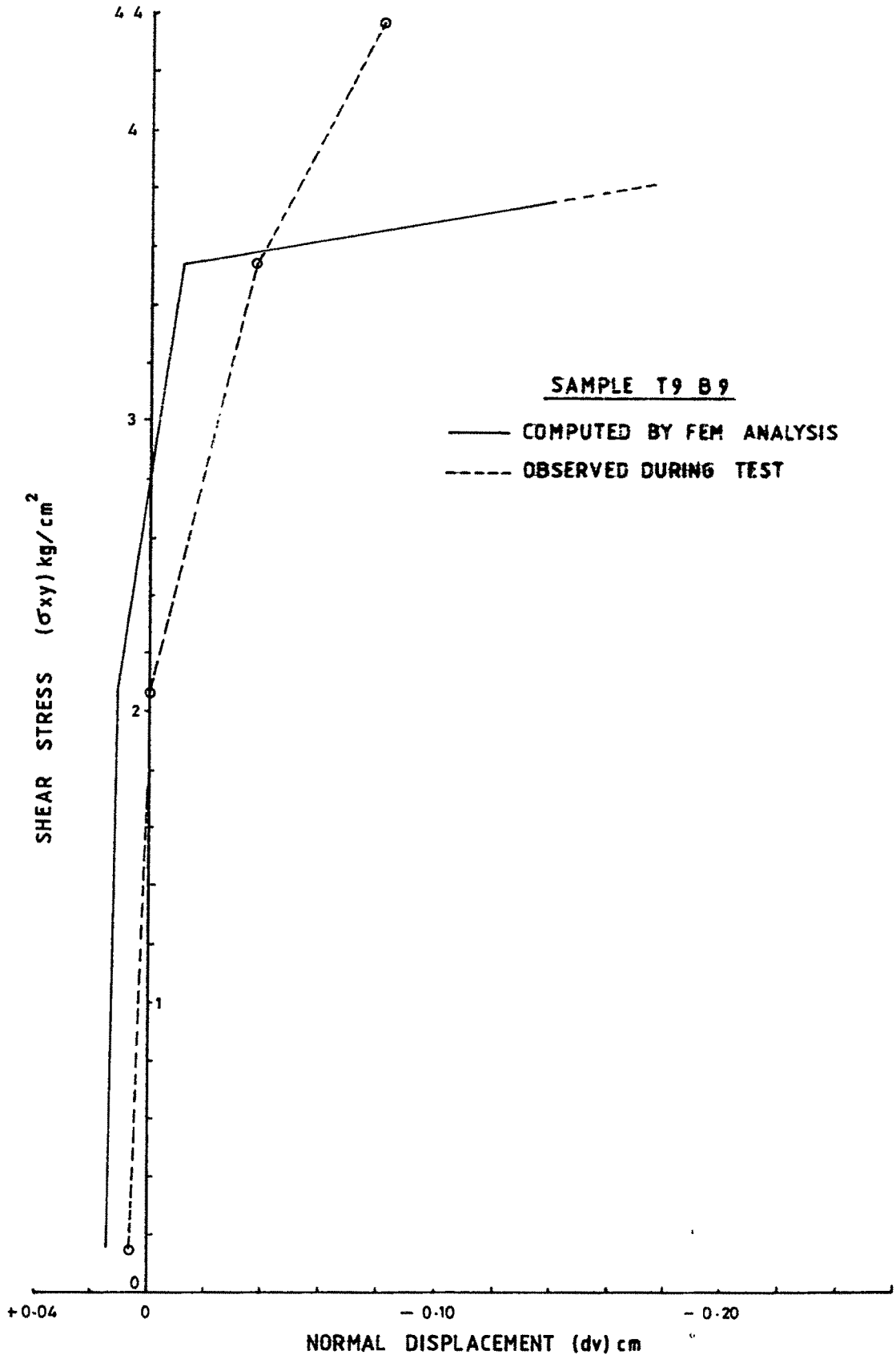

FIG: 7·32 COMPARISION OF COMPUTED AND OBSERVED DISPLACEMENTS

REGULARLY ASPIRATED SURFACES

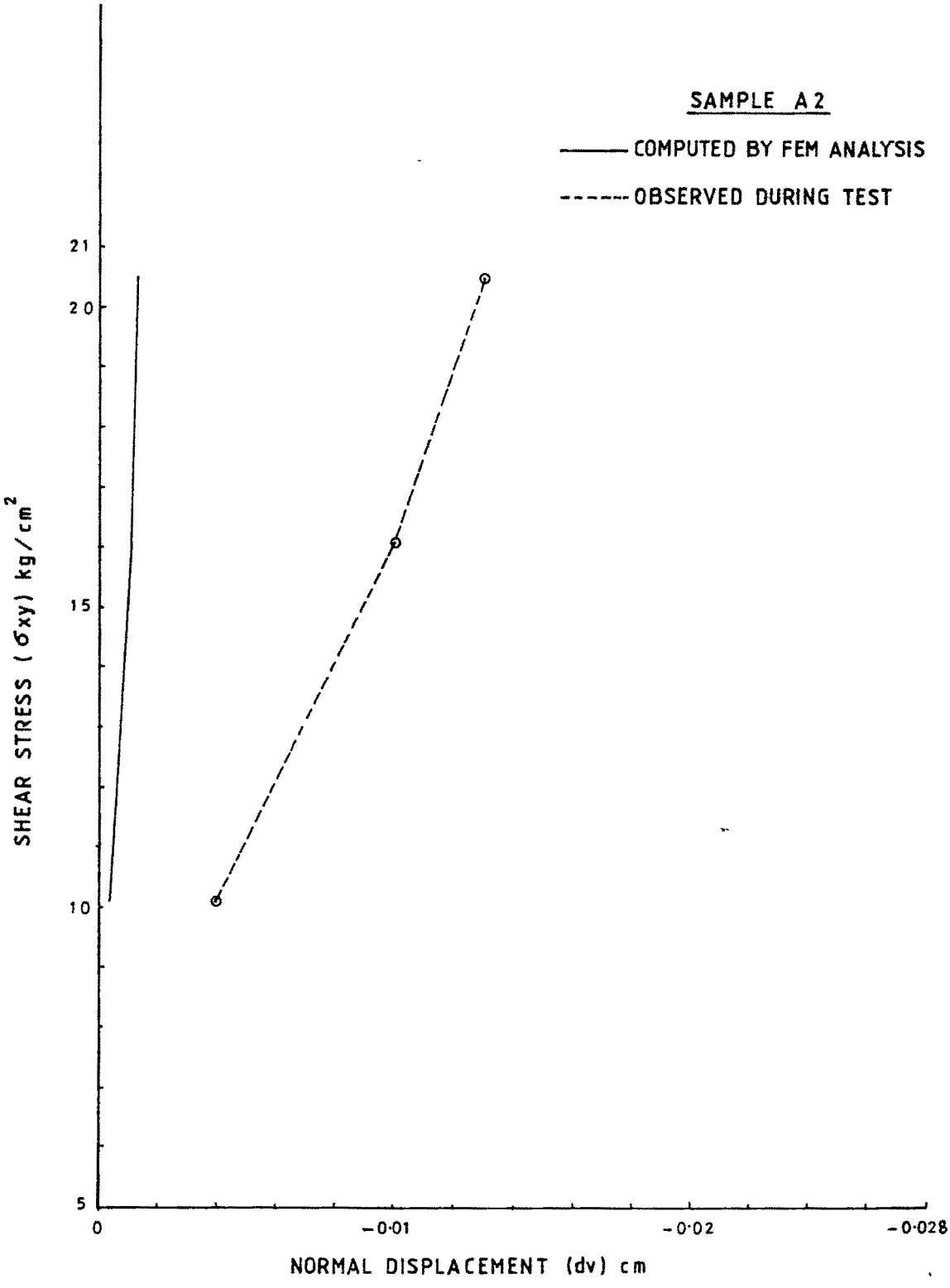

FIG: 7·34 COMPARISION OF COMPUTED AND OBSERVED DISPLACEMENTS

- DAVE (1987)

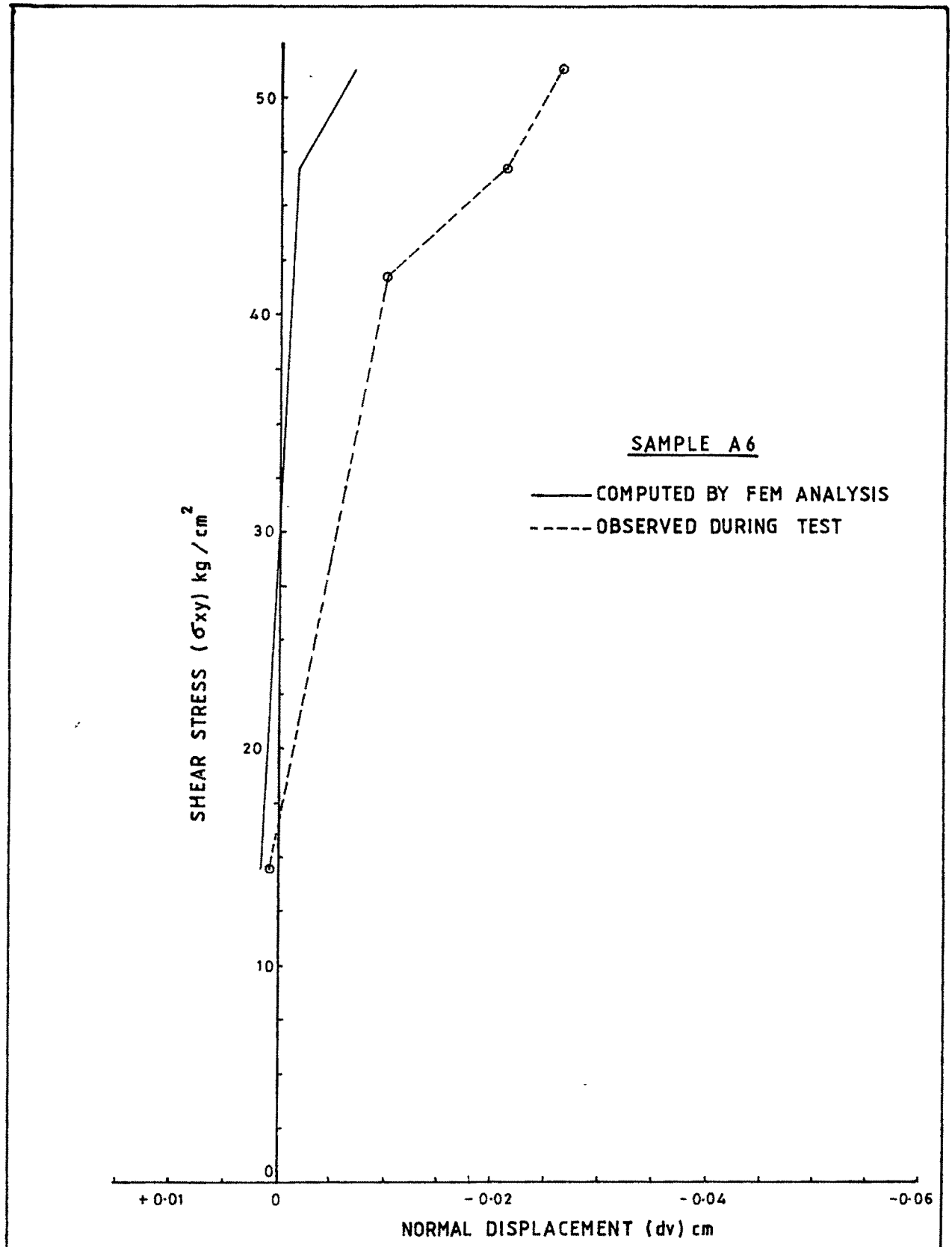

FIG 7·35 COMPARISION OF COMPUTED AND OBSERVED DISPLACEMENTS

- DAVE (1987)

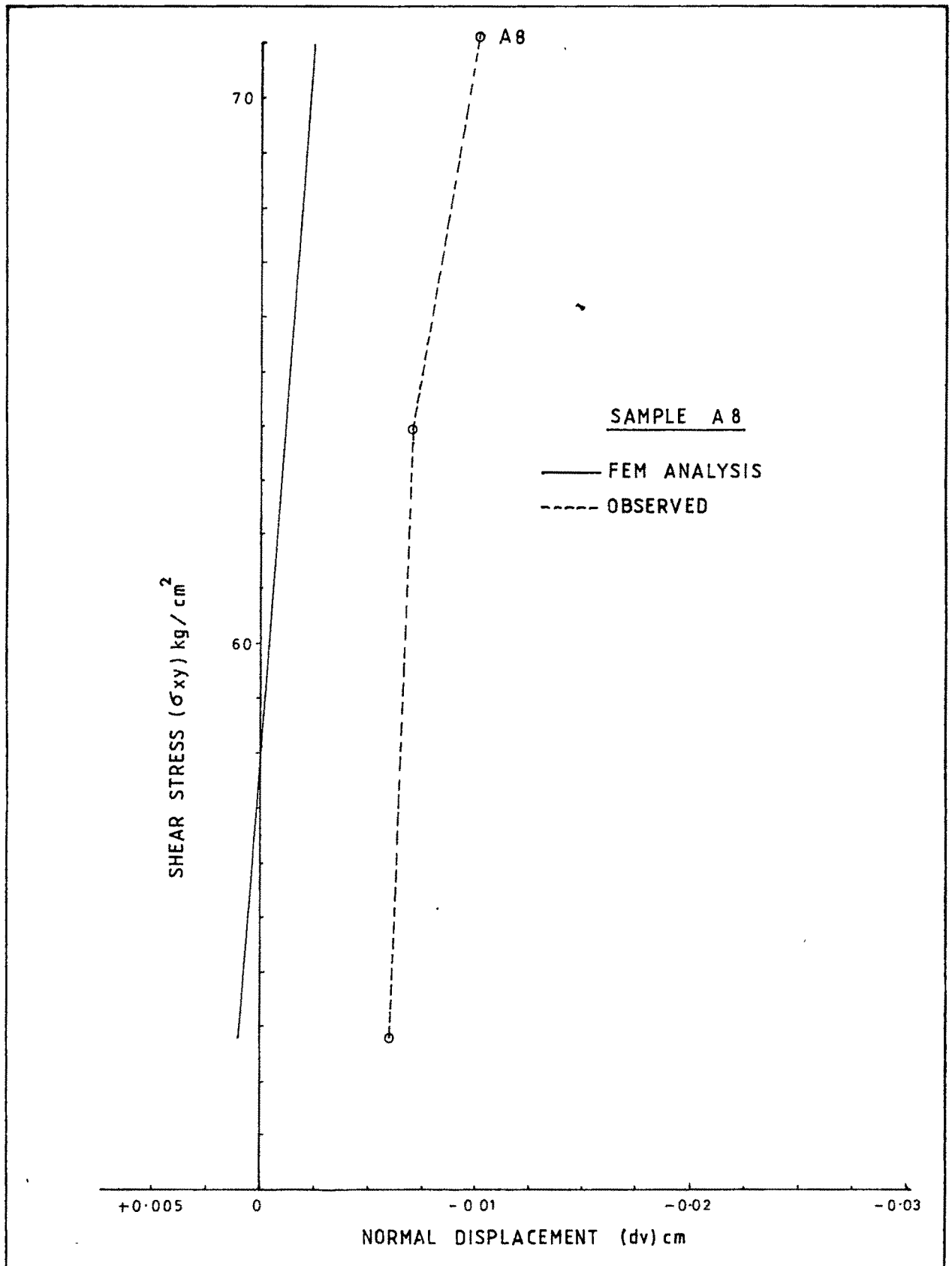

FIG 7·36 COMPARISION OF COMPUTED AND OBSERVED DISPLACEMENTS

-DAVE (1987)

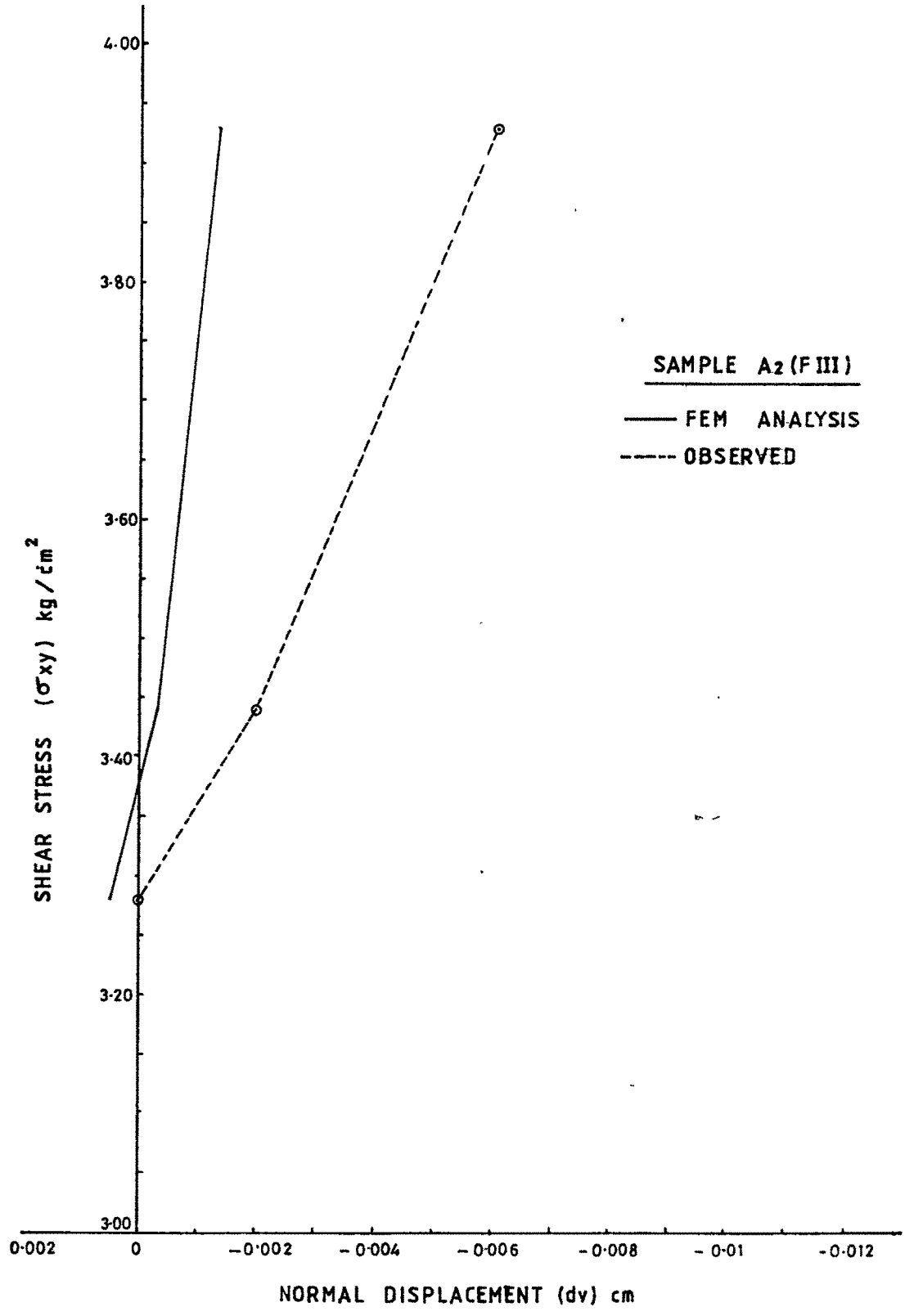

+FIG: 7·37 COMPARISION OF COMPUTED AND OBSERVED DISPLACEMENTS

-SHAH (1987)

7.38. The trend are similar in observed and computed values as in case of Dave (1987). The reason for difference in numerical values is same as discussed in case of Dave (1987).

7.6.5 Insitu Shear Tests conducted by Datir (1981)

The insitu test block is discretized as shown in Fig. 7.39. An average asperity angle is estimated to be 36°. Therefore a geometrical asperity of this angular value is introduced in the joint element as shown in the figure. Values of G, ν and E are obtained as discussed in previous cases. Observed and computed values of normal displacements have been plotted versus shear stress and presented in Fig. 7.40 to 7.42 which indicate a close conformity.

7.6.6 Case of a Single Element (Desai et al (1984))

Desai and Zaman (1984) have discussed application of a thin layer interface element developed by them to single element shown in Fig. 7.43, considering linear elastic material. The linear elastic material properties assumed are :

$$E = 1000 \text{ units}$$

$$\nu = 0.3$$

$$G = 10 \text{ units}$$

Dimensions of the element and loading are shown in the figure. Results computed by them are shown in Table 7.11. It is claimed that the computed shear stress is very close to the applied shear stress, and the computed displacements at the top nodes are close to the exact solution.

The new joint element is analysed by the FEM programme discussed earlier incorporating the developed constitutive

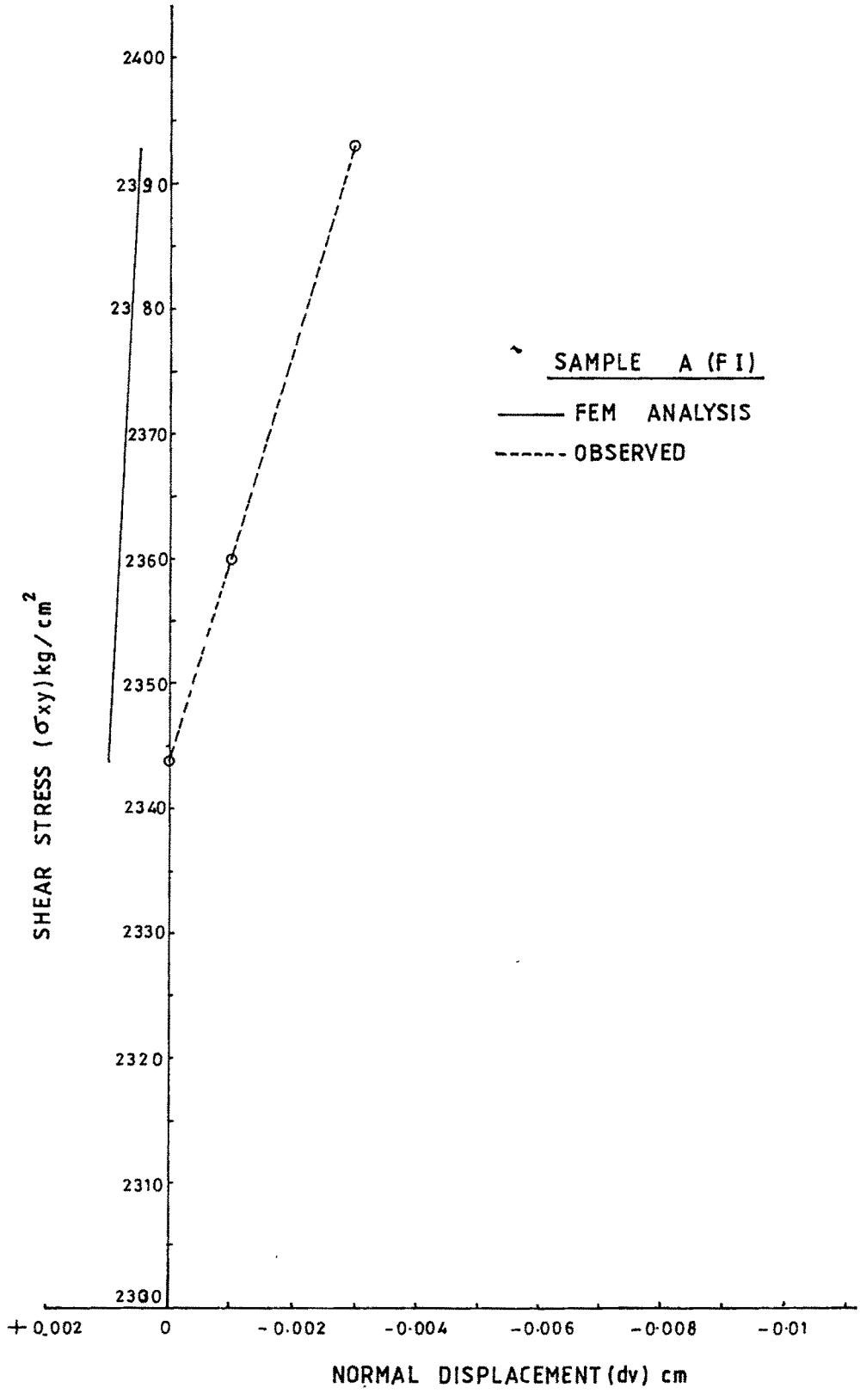

FIG: 7·38 COMPARISION OF COMPUTED AND OBSERVED DISPLACEMENTS

- SHAH (1987)

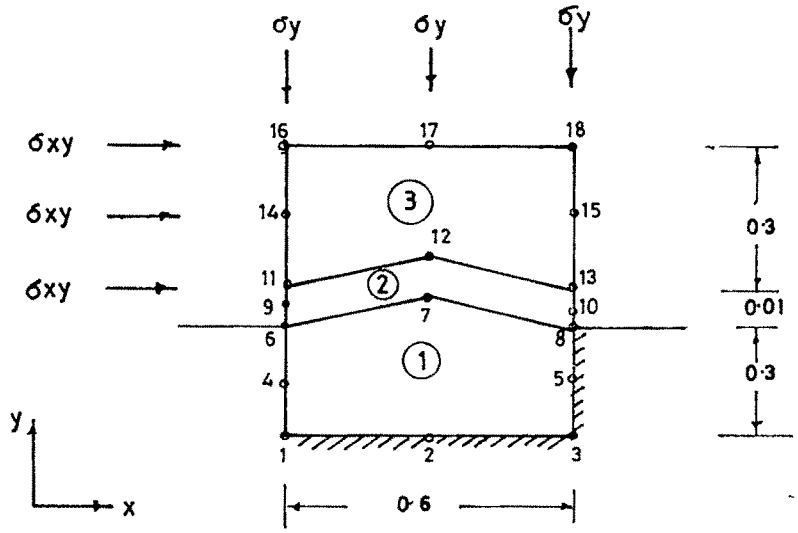

FIG: 7·39 DISCRETIZATION OF INSITU SHEAR TEST BLOCK

– DATIR (1981)

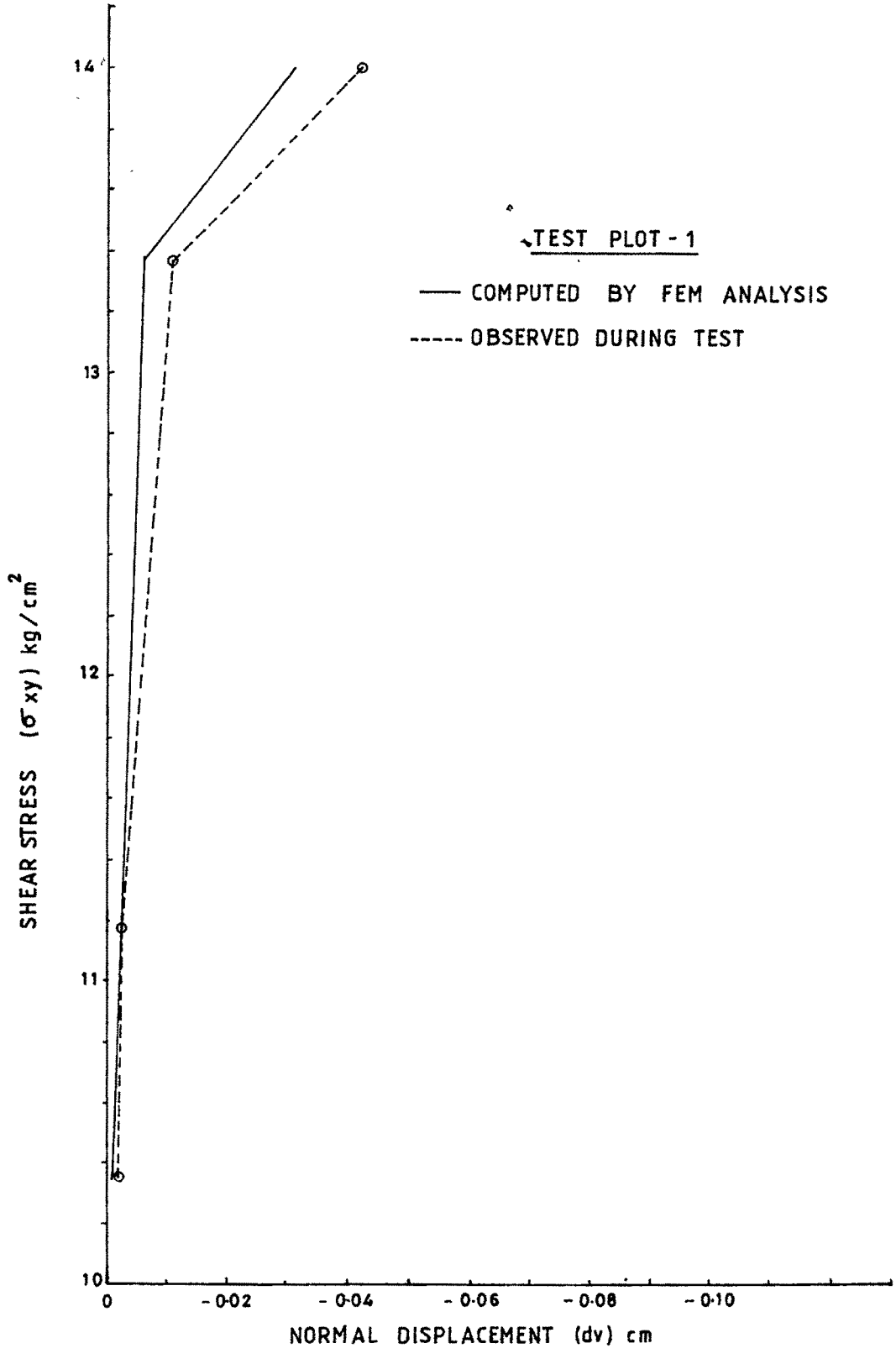

FIG: 7·40 COMPARISION OF COMPUTED AND OBSERVED DISPLACEMENTS

– DATIR · (1981)

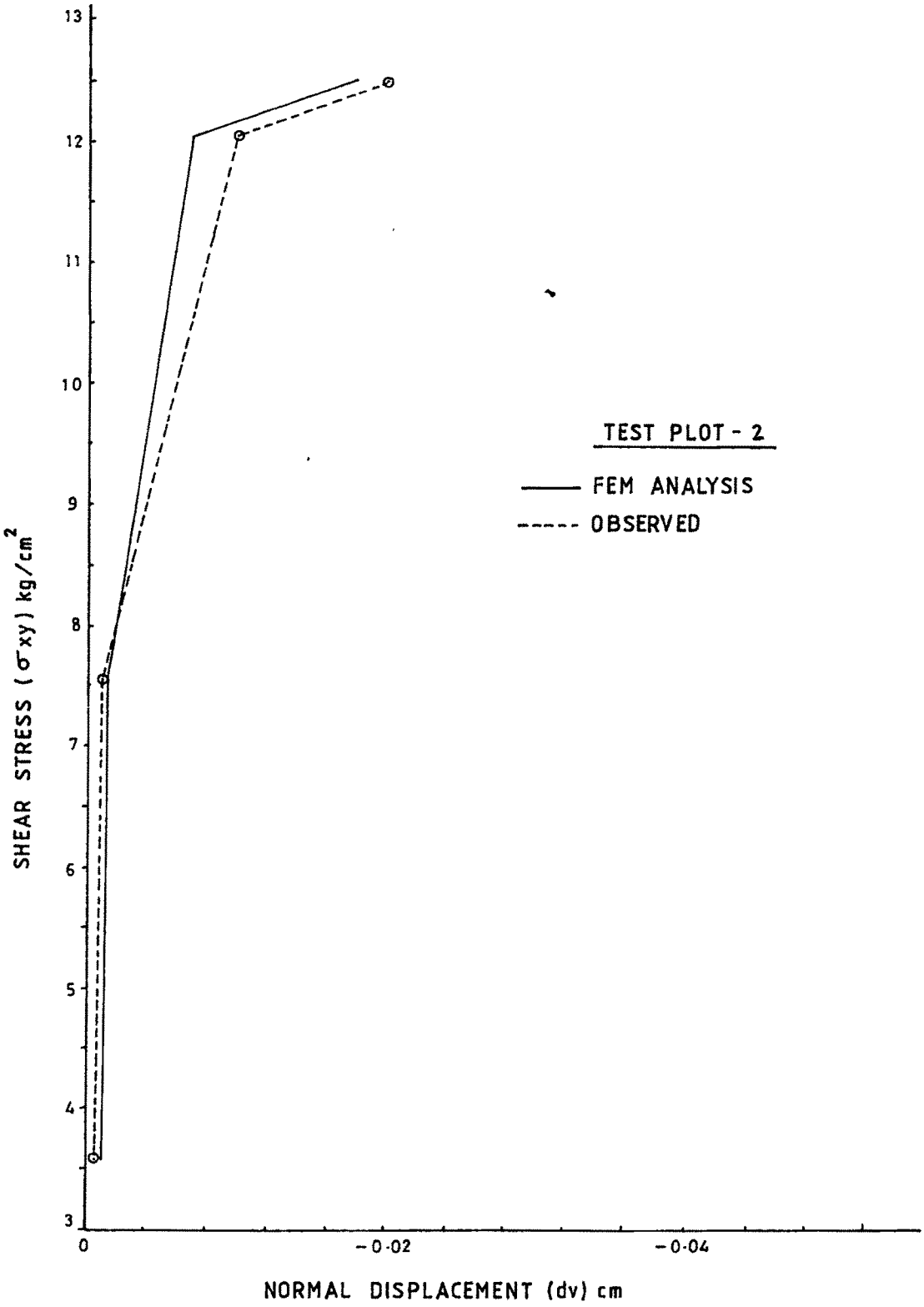

FIG: 7·41 COMPARISION OF COMPUTED AND OBSERVED DISPLACEMENTS

- DATIR (1981)

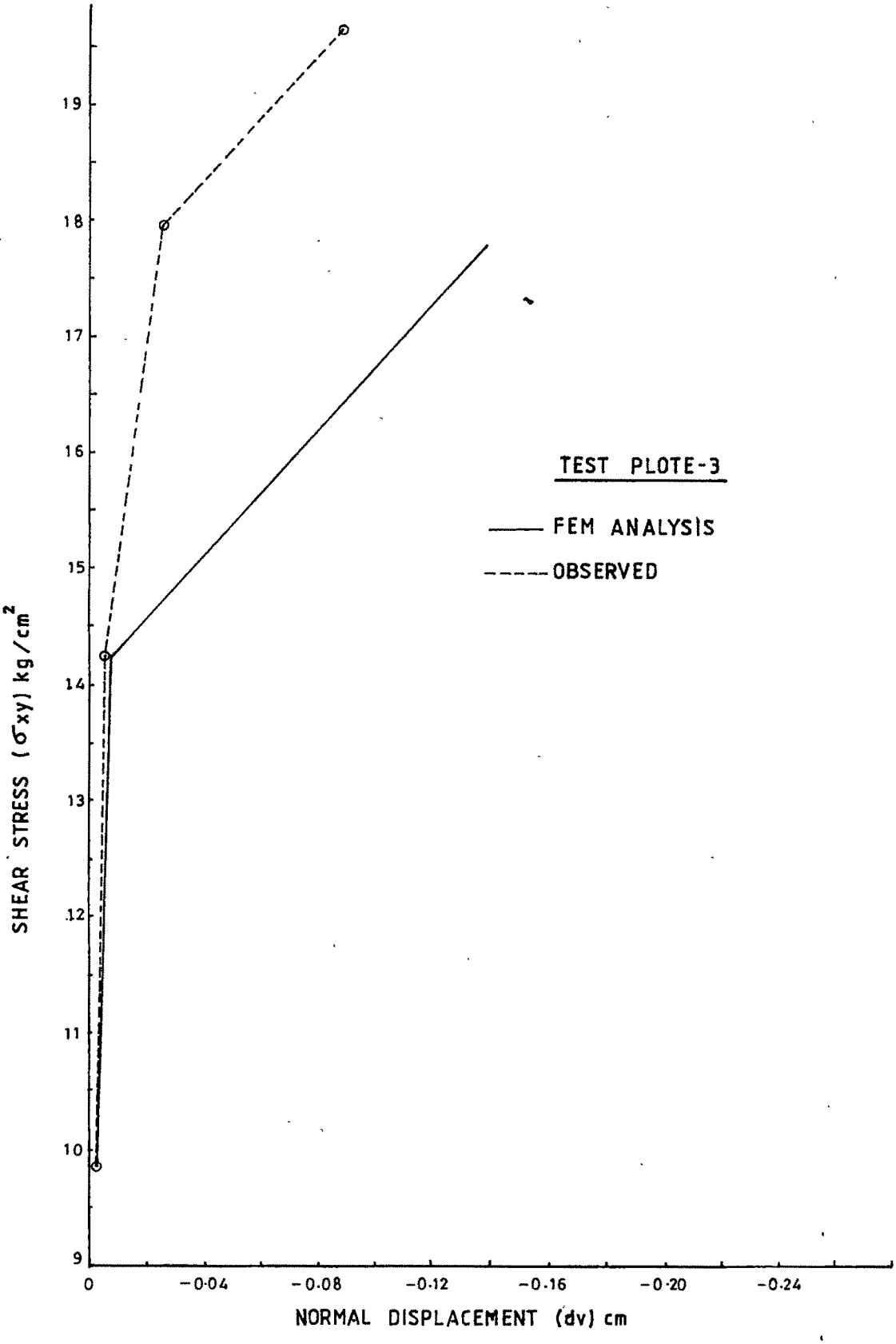

FIG 7 42 COMPARISION OF COMPUTED AND OBSERVED DISPLACEMENTS

-DATIR (1981)

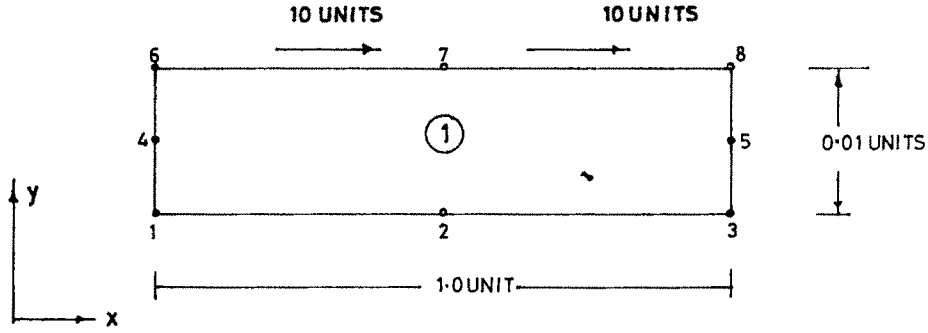

FIG: 7·43 SINGLE JOINT ELEMENT FOR LINEAR BEHAVIOUR

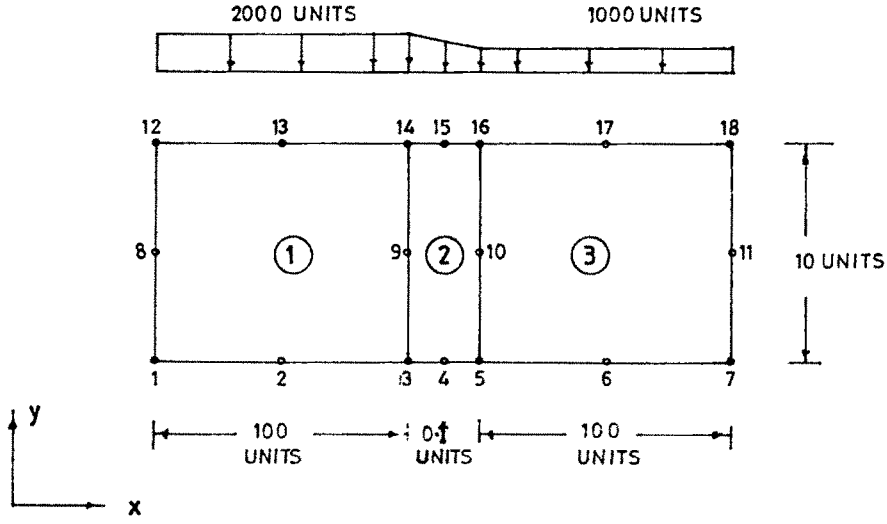

FIG: 7·44 TWO DIMENSIONAL CASE LINEAR ELASTIC BEHAVIOUR

TABLE 7.11 : CASE OF A SINGLE ELEMENT

Gauss Point No.	Shear stress reported by Desai et al (1984)	Shear stress computed for		
		ν =0.3	ν =0.99	ν =1.5
1	10.00350	10.0000	10.0000	9.9985
2	9.99825	10.0000	10.0000	9.9985
3	10.00350	10.000	10.000	9.9985
4	10.00350	9.9994	10.0000	10.0020
5	10.00350	9.9994	10.0000	10.0000
6	10.00350	10.0000	10.0000	9.9985
7	9.99835	10.0000	10.0000	9.9985
8	10.00350	10.0000	10.0000	9.9985

Node No.	Normal displacement reported by Desai et al (1984) $X10^{-4}$	Normal displacement computed for $X10^{-4}$		
		ν =0.3	ν =0.99	ν =1.5
1	0.00000	0.00000	0.00000	0.00000
2	0.00000	0.00000	0.00000	0.00000
3	0.00000	0.00000	0.00000	0.00000
4	1.68272	3.83037	0.101916	-6.84017
5	-1.68272	-3.83037	-0.101916	6.84017
6	2.27373	5.10720	0.135888	-9.12001
7	0.00000	0.00000	0.00000	0.00000
8	-2.27373	-5.10720	-0.135888	9.11998

Node No.	Shear displacement reported by Desai et al (1984) $X10^{-2}$	Shear displacement computed for $X10^{-2}$		
		ν =0.3	ν =0.99	ν =1.5
1	0.00000	0.00000	0.00000	0.00000
2	0.00000	0.00000	0.00000	0.00000
3	0.00000	0.00000	0.00000	0.00000
4	0.500177	0.769444	0.502518	0.399620
5	0.500177	0.769443	0.502518	0.399620
6	1.00035	1.53914	1.00504	0.798784
7	0.99827	1.53914	1.00504	0.798784
8	1.00035	1.53914	1.00504	0.798784

relationship given by equation 7.11. Keeping other data same, the value of ν is varied to represent compression, sliding and dilation, considering it in three stages as $\nu = 0.3$, $\nu = 0.99$ and $\nu = 1.5$. As discussed earlier, $\nu = 0.3$ indicates compressional mode, $\nu = 0.99$ (approximately equal to unity) corresponds to a stage of no volume change or the onset of dilation and , $\nu = 1.5$ indicates advance stage of dilation. A typical output from the computer analysis is given in Appendix-III. The computed values of Y displacements and shear stresses are compared with those reported by Desai et al (1984). These are incorporated in Table 7.11. It is seen from this table that for the stage of no volume change (i.e. $\nu = 0.99$), the distribution of shear stress is more even than reported by Desai et al (1984). The normal displacements are also almost negligible (very small in comparision to those reported by Desai et al (1984)). The shear displacements are similar to those reported by Desai et al (1984). For the stage corrresponding to $\nu = 0.3$ (compressional mode) the computed normal displacements are higher than those reported by Desai obviously because of compression. However, the nature of displacement at each node is same as reported by Desai. This means that normal displacements reported by Desai are for compressional mode. The distribution of shear stress is still even. The shear displacements are 1.5 times those at $\nu = 0.99$. For the stage corresponding to $\nu = 1.5$, the sign of the normal displacements are reverse than those at $\nu = 0.3$ and $\nu = 0.99$. This clearly indicates dilation. The values of normal displacements are much higher indicating an advance stage of dilation (under zero normal stress considered in the problem). The distribution of shear stress is not as even as that at $\nu = 0.3$ and $\nu = 0.99$, but the distribution is still considerably even. The shear displacements are smaller than those at $\nu = 0.3$ and $\nu = 0.99$ indicating that during shearing with dilation the shear displacements would be smaller than those during shearing without dilation or without volume change and this is obvious too.

Thus, the concept of variation in Poisson's ratio is

proved and the consitutive matrix developed during the present investigation has been tested to prove its ability to compute logical results which are also comparable with those reported in the literature.

7.6.7 Two Dimensional Case (Desai et al (1984))

Desai and Žaman (1984) have discussed application of thin layer interface element developed by them to two dimensional case shown in Fig. 7.44, considering linear elastic behaviour. Geometry and loading are shown in the Figure. The properties of the solid and interface elements considered are as under :

Solid elements	Interface element
E = 10000 psi	E = 1000 psi
ν = 0.3	ν = 0.3
	Gi = 20 psi

The results of vertical displacement of two typical points A and B computed by them are given in Fig. 7.45. The problem is analysed with the new joint element and its constitutive matrix. Keeping other data same, value of ν has been changed as ν = 0.3, ν = 0.99 and ν = 1.5. The computed values are superimposed in Fig. 7.45. It can be seen that as discussed in the previous application, the shear displacement is minimum when ν = 1.5. Reasons for such behaviour are already discussed in previous para. Thus, in this application also, the developed joint element has computed logical values of displacements which are comparable with those reported by Desai et al (1984). There is, however, some difference in numerical values of displacements. This is probably due to the fact that the data input by Desai is in FPS system of units where as the FEM programme utilised in the present analysis accepted the same values in MKS units.

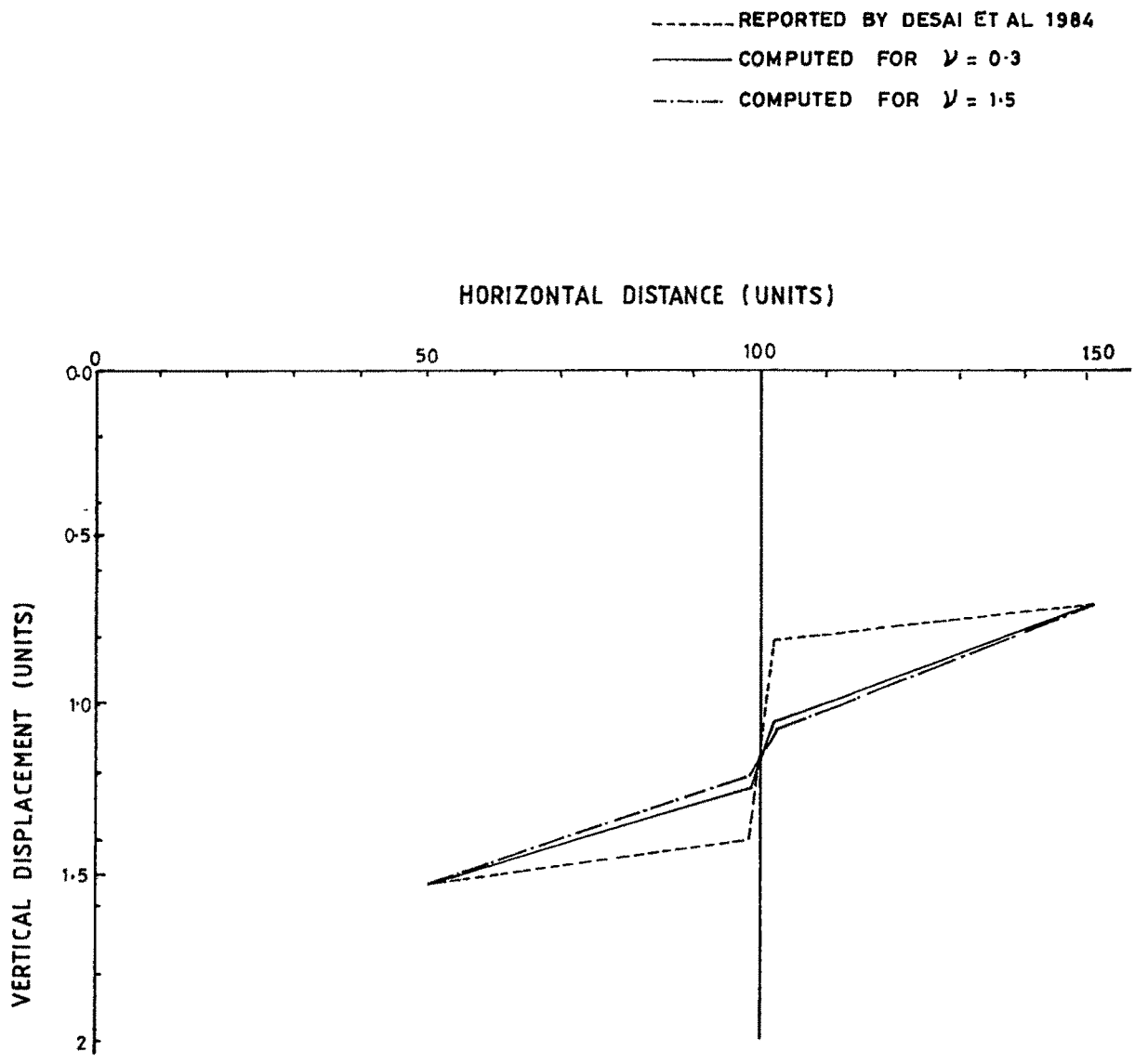

FIG: 7·45 TWO DIMENSIONAL CASE – COMPUTED DISPLACEMENTS

7.6.8 Case of Thick Circular Cylinder, typical of a Tunnel in a Jointed Rock, discussed by Hinton and Owen (1977)

Hinton and Owen (1977) have discussed a case of a thick circular cylinder. This is analogous to a circular opening in a jointed rock mass. The discretization used in the present analysis is shown in Fig. 7.46. A joint element is introduced in this discretization which was absent in the computations made by Hinton and Owen. The comparision of the two cases therefore directly gives the behaviour of the joint element. Radial stress distribution due to internal pressure loading along the centre line of the joint element is plotted in Fig. 7.47 as arrived at by Hinton and Owen (without joint element) and as arrived at in the present analysis (with joint element). It can be seen that for $\nu = 0.3$ the stress distribution reported by Hinton and Owen is comparable with stress distribution computed by the present analysis. Under this condition the stress concentration in the joint element near the face of the opening is 0.65. As ν increases to 0.99 the stress concentration falls down to 0.41. This is due to sliding without volume change. However, as ν increases beyond one, additional resistance to sliding is generated because of dilational mode and as a result, stress concentration increases to 0.80.

7.7 EFFICIENCY AND EFFICACY OF THE DEVELOPED JOINT ELEMENT

The joint element and its constitutive matrix developed in the present analysis have proved their applicability in the well accepted finite element programme. The constitutive matrix is first proved against the tests conducted on aspereted samples during the present investigation. Later on it is applied to laboratory direct shear, cyclic and insitu shear tests conducted by other investigators. The predicted behaviours are close to the observed one in most of the cases.

In order to prove the applicability of the joint element

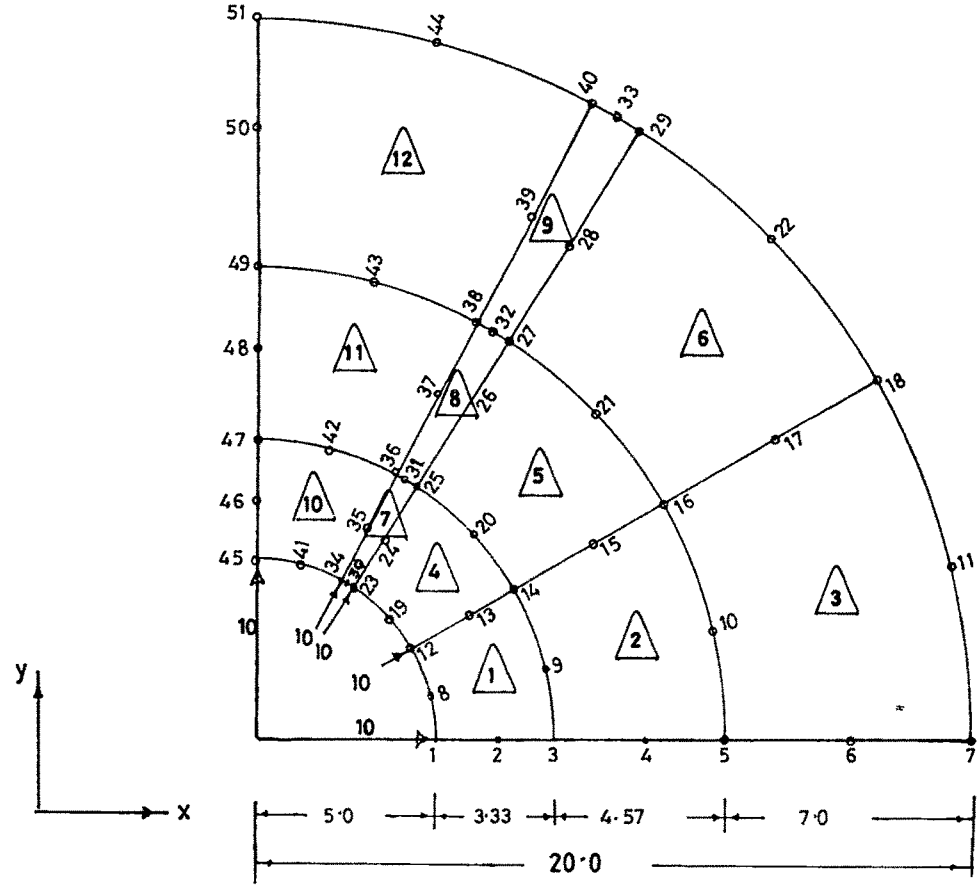

FIG: 7·46 DISCRETIZATION FOR CIRCULAR OPENING IN A JOINTED ROCK WITH INTERNAL PRESSURE

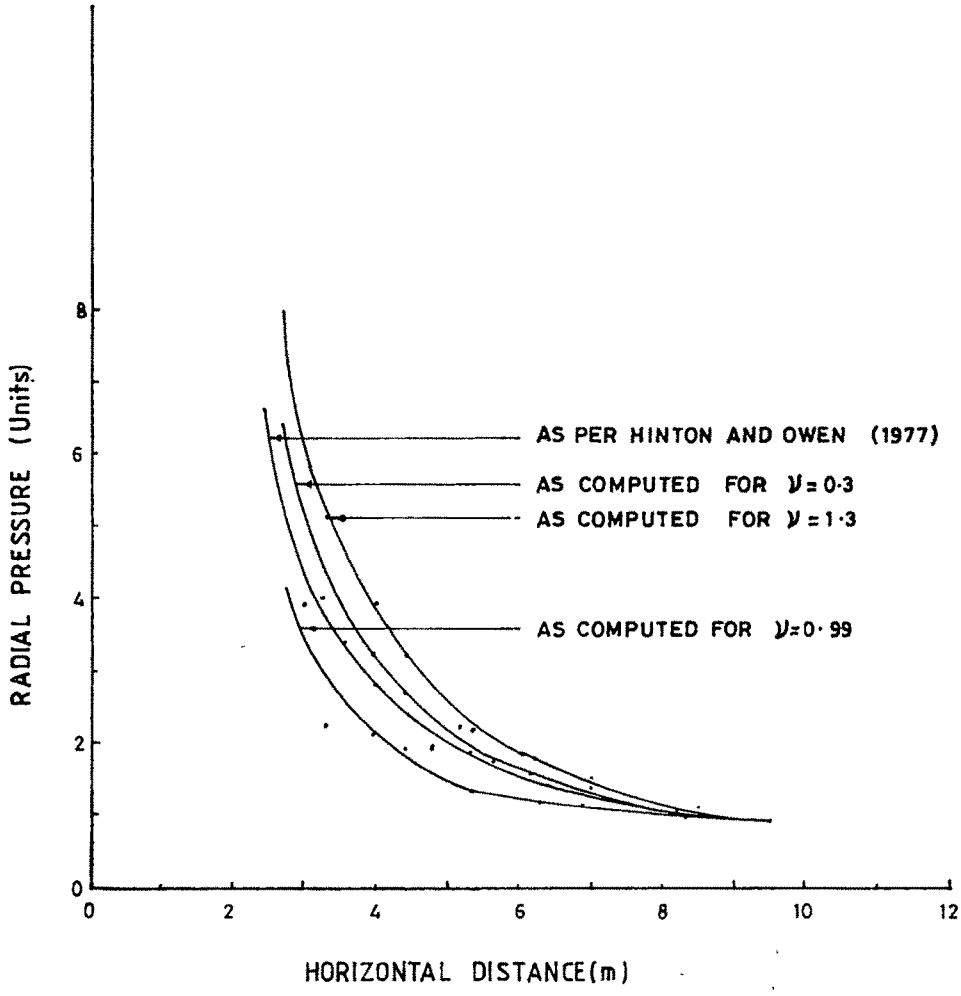

FIG: 7.47 RADIAL STRESS DISTRIBUTION ALONG JOINT ELEMENT

developed, it is incorporated in the 2D plane stress/plane strain Finite Element Programme developed by Hinton and Owen (1977). The same is then applied to the test data of laboratory direct shear, cyclic and insitu shear tests. The joint element has not only proved its applicability beyond doubt but has also predicted displacements comparable (and in most of the cases close) to the observed one.

The joint element is later on applied to two hypothetical cases reported by Desai et al (1984) and one reported by Hinton and Owen (1977). In all the cases the joint element and the constitutive matrix have proved their ability in predicting logical and meaningful behaviour. Thus the efficiency and efficacy of the developed joint element are self evident.

7.8 CONCLUSIONS

Significant conclusions that accrues from the analysis are summarized as under :

(i) The classical laws are followed in case of sliding on plane surfaces, whether lubricated or unlubricated, while deviation from the classical laws of friction is observed in case of sliding over aspirated surfaces. The deviation is a consequence of volume change occurring during sliding. The classical friction equations, independent of volume change, therefore, need to be generalized by incorporating an appropriate parameter for volume change.

(ii) The generalized equation of sliding friction for all types of surfaces, shall be the integration of the classical sliding friction equation, rigorously true at every instant. The process of integration should include the consideration of distrotion of plane at every instant. The resultant distortion of plane at every instant of sliding can be accounted for in terms of a

geometrical parameter, consisting of ratio of principal strains, well known as Poisson's ratio in classical mechanics. The classical equation,

$$\tau = f(\mu, \sigma)$$

must have a generalized form of

$$\tau = f(\mu, \nu, \sigma)$$

(iii) The phenomenon of sliding on discontinuities in jointed rock is analogous to the phenomenon of sliding on aspirated surfaces. The sliding in jointed rock therefore, is associated with continuous alterations of surface characteristics. In physical terms, the process of sliding is occurring at new plane of orientation continuously. The phenomenological parameter representative of the alteration of surface characteristics has been identified in terms of change of Poisson's ratio at every instant.

(iv) The operative equation to describe the sliding behaviour in jointed rock as deduced from the experimental observations in laboratory as well as in field is,

$$\tau = \sigma^{\cos i_o} \tan(\phi_\mu + i_o)$$

Alternatively,

$$\tau = \sigma \tan(\phi_\mu + i_{av})$$

where,

$$i_{av} = \tfrac{2}{3} i_o \, \sigma^{-\tan^2(45 - \phi_\mu/2)}$$

(v) A new joint element has been developed from the basic phenomenon of sliding in jointed rock, by incorporating change in Poisson's ratio at every instant in the constitutive matrix. The constitutive matrix can be given in the following forms :

$$(D) = \frac{1}{E}\begin{bmatrix} 1 & 0 & 0 \\ 0 & 1-\nu^2 & 1-\nu \\ 0 & 0 & 1+\nu \end{bmatrix}$$

Alternatively,

$$(D) = \frac{1}{E}\begin{bmatrix} 1 & 0 & 0 \\ 0 & 2D(1-\nu)(1+2\nu) & 0 \\ 0 & 0 & 1+\nu \end{bmatrix}$$

(vi) The developed joint element has a utility as a solid element in a finite element method. The utility has been demonstrated in predicting the behaviour of jointed rocks observed in laboratory as well as in field as also in engineering situations.

(vii) The efficiency and efficacy of the proposed new joint element has been established by realistic predictions of not only the generalized parameters of stresses and displacements but also the particular parameter associated with volume change, which is the distinguishing characteristics of the mechanical behaviour of jointed rock.

(viii) The superiority of the new element developed during this investigation is the incorporation of the phenomenological parameter of dilation in terms of change in Poisson's ratio, consequent upon which it is possible to delineate various deformation modes like compression, sliding and dilation.

In bravity, the mechanical behaviour of jointed rock can be realistically predicted only if the phenomenon of dilation is appropriately incorporated in the constitutive relationship.